Membrane tension controls adhesion positioning at the leading edge of cells

Bruno Pontes,[1,2] Pascale Monzo,[1,3] Laurent Gole,[1] Anabel-Lise Le Roux,[4] Anita Joanna Kosmalska,[4] Zhi Yang Tam,[1] Weiwei Luo,[1] Sophie Kan,[1] Virgile Viasnoff,[1,5] Pere Roca-Cusachs,[4,6] Lisa Tucker-Kellogg,[1,7] and Nils C. Gauthier[1,3]

[1]Mechanobiology Institute, National University of Singapore, Singapore
[2]Laboratório de Pinças Óticas, Instituto de Ciências Biomédicas, Universidade Federal do Rio de Janeiro, Rio de Janeiro, Brazil
[3]Institute FIRC (Italian Foundation for Cancer Research) of Molecular Oncology (IFOM-FIRC), Milan, Italy
[4]Institute for Bioengineering of Catalonia, The Barcelona Institute of Science and Technology, Barcelona, Spain
[5]Centre National de la Recherche Scientifique, École Supérieure de Physique et de Chimie Industrielles Paristech, Paris, France
[6]University of Barcelona, Barcelona, Spain
[7]Centre for Computational Biology, Duke–National University of Singapore Graduate Medical School, Singapore

Cell migration is dependent on adhesion dynamics and actin cytoskeleton remodeling at the leading edge. These events may be physically constrained by the plasma membrane. Here, we show that the mechanical signal produced by an increase in plasma membrane tension triggers the positioning of new rows of adhesions at the leading edge. During protrusion, as membrane tension increases, velocity slows, and the lamellipodium buckles upward in a myosin II–independent manner. The buckling occurs between the front of the lamellipodium, where nascent adhesions are positioned in rows, and the base of the lamellipodium, where a vinculin-dependent clutch couples actin to previously positioned adhesions. As membrane tension decreases, protrusion resumes and buckling disappears, until the next cycle. We propose that the mechanical signal of membrane tension exerts upstream control in mechanotransduction by periodically compressing and relaxing the lamellipodium, leading to the positioning of adhesions at the leading edge of cells.

Introduction

Cell migration is dependent on adhesion dynamics and cytoskeleton remodeling at the leading edge, or lamellipodium. Lamellipodial protrusion is driven by actin polymerization that pushes the plasma membrane forward. In this fast actin-reorganizing structure, the force exerted by cytoskeleton polymerization results in the formation of a retrograde actin flow opposite to membrane protrusion (Theriot and Mitchison, 1991; Pollard and Borisy, 2003; Le Clainche and Carlier, 2008). This flow is counteracted by integrin-based adhesions on the substrate, resulting in protrusive forces (Prass et al., 2006). The formation of adhesions is now understood to be myosin II independent, whereas myosin II–mediated contraction is required for maturation of early adhesions into larger focal adhesions (Choi et al., 2008; Parsons et al., 2010). The mechanical link between the lamellipodium and adhesions is proposed to occur through a molecular "clutch" that engages actin with integrins (Hu et al., 2007). Vinculin is one of the major components of this clutch: it attaches to the actin mesh and to integrin receptors through direct binding and through adaptor proteins such as talin (Thievessen et al., 2013; Case et al., 2015). As a consequence, vinculin provides a mechanotransduction cascade linking actin forces to adhesion dynamics.

Because the plasma membrane is the leading structure to be pushed forward in the lamellipodium, it is reasonable to think that the plasma membrane can also exert a counterbalancing force against the lamellipodial actin. This force per unit length is the membrane tension (Keren, 2011; Gauthier et al., 2012; Diz-Muñoz et al., 2013; Pontes et al., 2013). Membrane tension has been described to constrain lamellipodial protrusion, with high tension decelerating protrusion and low tension facilitating protrusion (Raucher and Sheetz, 2000; Gauthier et al., 2011; Masters et al., 2013; Tsujita et al., 2015). Membrane tension is also key for lamellipodial organization in cells that do not use actin for protrusion, such as nematode sperm cells (Batchelder et al., 2011). Moreover, membrane tension is critical for acquisition and maintenance of polarity in neutrophils, keratocytes, and macrophages (Houk et al., 2012; Lieber et al., 2013, 2015; Masters et al., 2013; Diz-Muñoz et al., 2016). However, despite some computational modeling–based inferences (Ji et al., 2008; Shemesh et al., 2012; Schweitzer et al., 2014), little is known about the cytoskeletal phenomena triggered by membrane tension changes or the effects regulating adhesion dynamics. It is worth noting that the computational model by Shemesh et al. (2012) proposed that upon an increase in membrane tension,

Correspondence to Nils C. Gauthier: nils.gauthier@ifom.eu

Abbreviations used: BBI, blebbistatin; DIC, differential interference contrast; epi, epifluorescence; hypo-OS, hypo-osmotic shock; PDMS, polydimethylsiloxane; tirf, total internal reflection fluorescence; VASP, vasodilator-stimulated phosphoprotein.

The Rockefeller University Press
J. Cell Biol. Vol. 216 No. 9 2959–2977
https://doi.org/10.1083/jcb.201611117

the dynamics of protrusion can switch behaviors and lead to a narrower lamellipodial region with adhesions at its rear.

Previous studies described a robust increase in plasma membrane tension that occurs transiently during mouse embryonic fibroblast (MEF) cell spreading on fibronectin-coated substrate and frustrated phagocytosis of macrophages on immunoglobulin-coated substrate (Gauthier et al., 2011, 2012; Masters et al., 2013). This increase in tension is consistently observed during the transition (T) between the fast early spreading phase (P1) and the later oscillatory phase of spreading (P2). P1 is characterized by an isotropic spreading with unfolding of plasma membrane reservoirs, whereas P2 is characterized by slow, periodic spreading with exocytic transport of lipid membranes to the cell surface (Gauthier et al., 2011, 2012; Fig. 1 A, schematic). During T, when membrane tension temporarily increases, there is a decrease in cell edge velocity, followed by progressive shortening of the lamellipodium and actin reinforcement at the cell edge (Dubin-Thaler et al., 2004, 2008; Gauthier et al., 2011; Masters et al., 2013). When membrane tension subsequently decreases, the cell edge resumes protrusion (Gauthier et al., 2011).

During P2, cell adhesions mature in a myosin II–dependent manner and are cyclically positioned in rows (Giannone et al., 2004, 2007). Oscillating cycles have also been reported to be a key feature for migration in numerous cell types, including epithelial cells (Burnette et al., 2011), endothelial cells (Giannone et al., 2004, 2007), and MEFs (Giannone et al., 2004, 2007; Machacek et al., 2009; Burnette et al., 2011). The capacity of the edge to oscillate is highly robust, but the period of oscillation, ranging from tens of seconds to a few minutes, depends on the cell type (Giannone et al., 2004, 2007; Machacek et al., 2009; Burnette et al., 2011; Doyle et al., 2012). For the fibroblasts used in this study, the period ranges between 15 and 30 s (mean of ∼24 s), with the protrusions lasting ∼19 s and the retractions lasting ∼5 s (Giannone et al., 2004, 2007; Gauthier et al., 2011). However, little is known about how membrane tension behaves during P2 or during P2-like oscillatory cycles of cell migration. Moreover, it is also unknown how and whether membrane tension changes could affect adhesion dynamics during all spreading phases and also in fibroblast polarized migration.

Here we investigate how changes in membrane tension influence the actin cytoskeleton and adhesion behaviors in the lamellipodium, explicitly decoupling the events that are sensitive to membrane tension from those that are myosin II dependent. Our results demonstrate that an increase in membrane tension exerts an upstream control in mechanotransduction by physically constraining the lamellipodium. Subsequently, the lamellipodium acts as a mechanotransducer, transmitting the membrane tension loads to the substrate and rearranging and positioning adhesions in the leading edge in a myosin II–independent but vinculin-dependent manner.

Results

Adhesion positioning is spatiotemporally correlated with a temporary increase in membrane tension during the P1/P2 transition of cell spreading

Actin and vasodilator-stimulated phosphoprotein (VASP) were followed by time-lapse total internal reflection fluorescence (tirf) microscopy (a complete list of constructs used in this study is presented in Materials and methods), allowing us to track their behaviors during MEF spreading (Fig. 1). VASP is known to be present both in adhesions and at the tip of the leading edge of cells (Lacayo et al., 2007; Dubin-Thaler et al., 2008; Trichet et al., 2008). As expected, we observed VASP in adhesion clusters located at the back of lamellipodia, colocalized with actin foci (Fig. 1 B).

During the P1 phase of spreading, new clusters of adhesions were positioned in stagger locations and timings (Fig. 1 B and Video 1). Strikingly, a nearly constant lamellipodial width of 5.2 ± 1.3 µm (between VASP adhesion clusters and cell edge) was maintained (Fig. 1, B, D, and H; and Video 1). However, at a certain point, there was a decrease in cell edge velocity followed by progressive shortening of the lamellipodium and actin reinforcement at the cell edge. At this stage, membrane tension temporarily increased, as previously reported (Gauthier et al., 2011), because the spreading cell reached the transition T (Fig. 1, B–D and G–I; and Video 1). Moreover, VASP adhesion clusters became reinforced and started to become aligned in a row near the cell edge (Fig. 1 C), in effect moving the rear boundary of the lamellipodium outward and contributing to the dramatic decrease in lamellipodium width (from 5.2 ± 1.3 µm to 0.8 ± 0.4 µm; Fig. 1, B–D and G–I; and Video 1). After T, the spreading cell entered the P2 phase. The protrusion speed was slower than in P1 (Fig. 1, B and D). The adhesion clusters that were positioned during and after T matured into focal adhesions (Fig. 1, B and D). These focal adhesions appeared as horizontal strips in the kymograph (Fig. 1 D).

We next investigated the relation between the increase in membrane tension during T and the positioning of adhesions. We outlined the cell edge at the beginning of T, when it started to slow down (Fig. 1 E). We then superimposed the contour from phase T onto the image of the cell after adhesion maturation in P2. The first line of focal adhesions (from cell center to edge) that matured was positioned exactly at the locations where adhesions had aligned during T, when membrane tension is known to increase (Fig. 1 E). This observation suggests that the increase in membrane tension during T triggers the positioning of an adhesion row. Remarkably, this positioned row seemed to remain as a "memory" by the cell and matured into focal adhesions later during spreading (Fig. 1 E).

Simple kymographs, like the ones of Fig. 1 D, represent only a slice of the cell. To better quantify the entire process and estimate a mean value for the distance (D) between the clusters of adhesions and the cell leading edge during spreading, mean kymographs were generated (Fig. 1 H). These kymographs were created from the integration of mean intensity profiles (each one generated from the 360 different slices of a particular time point of the spreading cell, one per degree of rotation) and aligned by the cell edge (defined as the outermost point with actin fluorescence; Fig. 1 F). The position of adhesion clusters was defined as the outermost point with adhesion marker fluorescence (Fig. 1 F). The mean intensity profiles (Fig. 1 G), the mean kymographs, and the mean kymograph plot (Fig. 1 H and Video 1) were obtained. The quantifications confirmed that D was larger during P1 and quickly decreased when the cell reached T (Fig. 1, H and I; and Video 1).

Finally, to further affirm the behaviors of adhesions over time, other known adhesion proteins were imaged in combination with actin during spreading. Integrin β3, paxillin, talin,

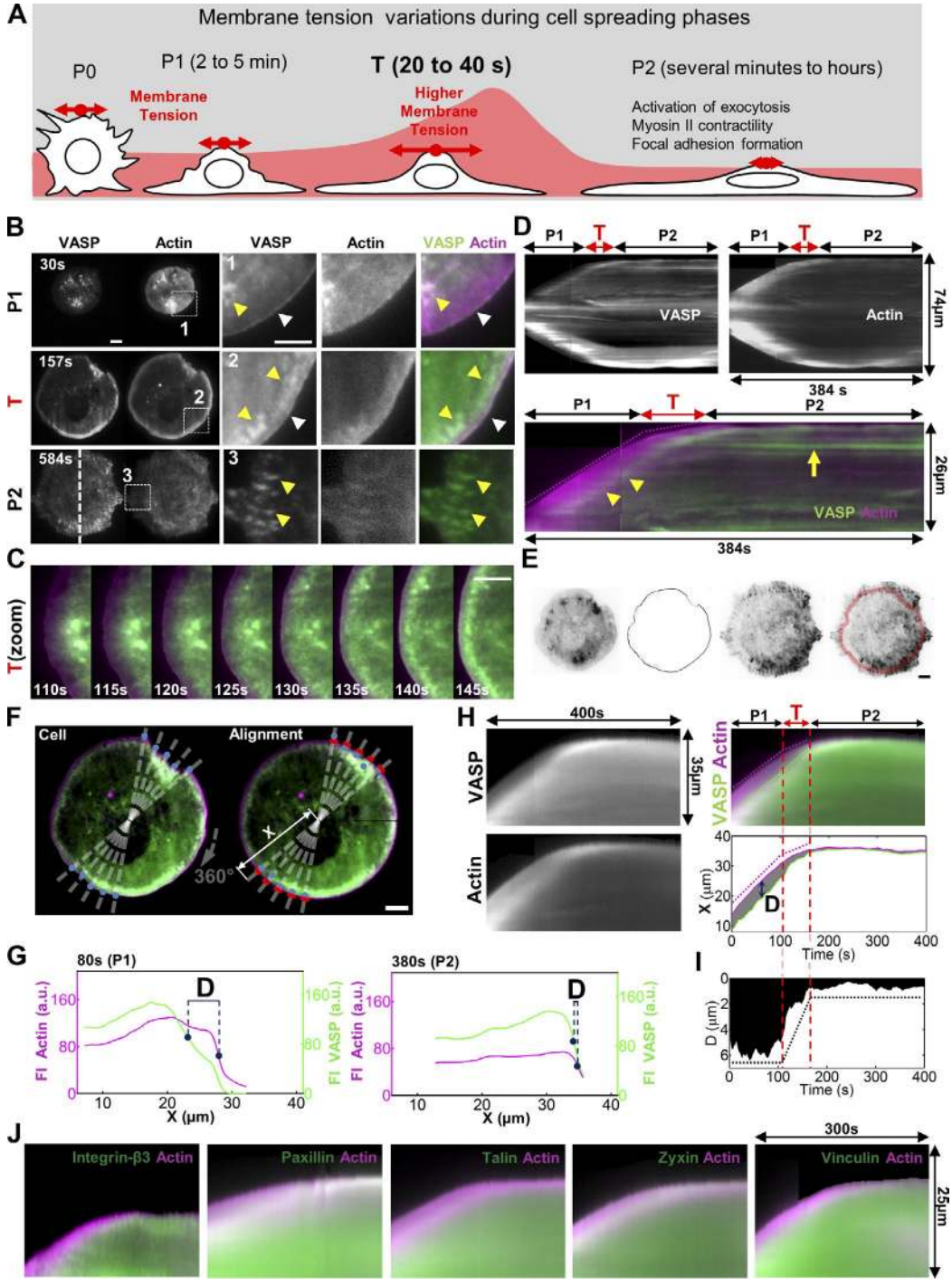

Figure 1. **Adhesion dynamics correlates with membrane tension changes during spreading.** (A) Cell spreading phases. Red arrows and curve, membrane tension. (B) VASP and actin during spreading. Dashed squares, zooms 1, 2, and 3; yellow arrowheads, VASP in clusters at the back of the lamellipodium; white arrowheads, VASP line at the tip of the leading edge. (C) Sequence of images showing VASP adhesion (green) dynamics relative to actin (magenta) during T. Lamellipodium decreases in size, and VASP adhesions organize as a row near the cell edge. (D) Kymograph of the cell presented in B (dashed line). Yellow arrowheads and arrow, VASP clusters in P1 and P2, respectively; magenta dashed curve, tangential guide to show the change in slope for the cell edge. (E) Row of adhesions positioned during T (increase in membrane tension) matures into focal adhesions later in P2, as indicated by the red outline (representing the adhesion row during T) superimposed with an image of the cell in late P2. (F) Procedure used to quantify adhesion positioning. Left, real frame of the cell; right, reconstructed cell; dashed lines, radius (*x*); blue dots, original edge position; red lines, aligned edge. (G) Representative mean intensity profiles for P1 and P2, with D (distance between the adhesion clusters and the cell edge) indicated. (H) Mean kymographs for VASP and actin and kymograph plot showing D (arrow in gray region). Magenta and green dashed lines, tangential guides to show the changes in slopes for the cell edge and adhesion clusters, respectively. Changes in slopes occur during T. (I) Variation of D during spreading. D changes from an initial ~6-µm plateau (P1) to a ~1-µm plateau (P2). T corresponds to the time necessary to change from one plateau to another (black dashed line, guide to show the change). (J) Mean kymographs for actin with other adhesion proteins. All procedures were repeated for at least 10 different spreading cells, and all showed behaviors similar to those represented in the figure. Bars, 10 µm.

zyxin, and vinculin behaviors (Video 2) resembled that of VASP and confirmed the substantial shortening of D during T (Fig. 1 J and Table 1).

In summary, the results suggest the existence of a spatiotemporal correlation between three phenomena that occur at the leading edge of spreading cells: (a) membrane tension increase during T; (b) shortening of the lamellipodium width; and (c) positioning of the first adhesion row.

Adhesion positioning is dependent on membrane tension but independent of myosin II

Adhesion positioning seems to be under membrane tension control. To obtain clearer evidence of such influence, we next decided to simulate an increase in tension and follow whether it is able to trigger adhesion positioning.

We first used a 50% hypo-osmotic shock (hypo-OS), treatment previously documented to increase membrane tension. Although we know that hypotonic stress may generate other side effects, it provides a quick and easy way to induce rapid changes in membrane tension, as already shown by several studies (Sinha et al., 2011; Houk et al., 2012; Masters et al., 2013; Tsujita et al., 2015; Diz-Muñoz et al., 2016).

We first checked whether the 50% hypo-OS was indeed inducing an increase in membrane tension in our system. For that, we extracted membrane tethers from MEFs with optical tweezers and followed the tether force over time, first when cells were in an isotonic medium (1× Ringer's) and then when they were changed to a hypotonic medium (0.5× Ringer's; Fig. 2, A and B). We measured these changes in single cells, as represented in Fig. 2 C. However, it is already known that tether forces can greatly vary between cells because of modifications in membrane composition and membrane-cytoskeleton attachments, so we also followed the tether force for each condition (1× and 0.5× Ringer's) in several other cells (Fig. 2 D). The results demonstrated that the tether force increased from 29 ± 1 to 38 ± 1 pN (~31% increase), representing a direct increase in membrane tension when MEFs are changed from isotonic to 50% hypotonic media.

Knowing that the hypo-OS is capable of inducing an increase in tension in our system, we next investigated whether this increase could simulate the normal tension increase that occurs during T. Before we answered this question, we followed actin and the adhesion protein paxillin during spreading in control cells using tirf time-lapse microscopy (Video 3). The results (Fig. 3, A–C; and Table 1) resembled the ones previously reported for VASP during all spreading phases.

When membrane tension was increased using a 50% hypotonic medium in a spreading cell between the middle and end of P1, when most of its membrane folds and ruffles were already depleted, the spreading immediately stopped and there was a rapid shortening of the lamellipodial width D (from 5.0 ± 1.3 to 0.5 ± 0.3 µm; Fig. 3, D–F; Video 3; and Table 1). The shortening of D was associated with the positioning of a clear row of paxillin close to the edge (Fig. 3 D and Video 3). This behavior simulated the normal transition T observed in control cells (Fig. 3 D compared with Fig. 3 A). Restoring isotonicity also restored membrane tension to previous values, as indicated by the formation of vacuole-like dilations (Video 3; Reuzeau et al., 1995; Morris and Homann, 2001; Gauthier et al., 2011; Masters et al., 2013; Kosmalska et al., 2015) and resumed spreading (Fig. 3, D and E; and Video 3). Remarkably, the row of adhesions positioned during the hypotonically elevated membrane tension was kept in memory by the cell and matured into focal adhesions later during spreading (Fig. 3, E and G). These results demonstrate that an artificial increase in membrane tension, between the middle and end of P1, is sufficient to simulate T by stalling and shortening lamellipodial protrusion and inducing actin reinforcement and adhesion row positioning at the cell edge.

Myosin II contractility was found to promote maturation of early adhesions into focal adhesions (Lo et al., 2004; Vicente-Manzanares et al., 2007). However, early adhesion dynamics was already described to be independent of myosin II (Choi et al., 2008; Parsons et al., 2010). After finding that elevated membrane tension was sufficient to induce positioning of a row of adhesions, we next asked whether membrane tension–mediated adhesion positioning also required myosin II contractility. Before spreading, MEFs were incubated with 10 µM blebbistatin (BBI) to inhibit myosin II activity (Straight et al., 2003). BBI-treated cells spread isotropically during P1 and T (Fig. 3, H–J; Video 3; and Table 1). In P2, BBI-treated cells were able to position rows of adhesion similarly to controls, but the rows never matured into focal adhesions (Fig. 3, H and I). Myosin II is therefore unnecessary for adhesion positioning during all spreading phases but essential for adhesion maturation in P2. We next artificially increased membrane tension, using a 50% hypotonic medium, in combination with myosin II inhibition. The behavior of cells resembled that during hypotonic treatment without BBI. When tension was artificially increased, the

Table 1. **Values of D for each experimental condition**

Adhesion molecules	*n*	D		
		P1	P2	hypo-OS
		µm	*µm*	*µm*
VASP	10	5.2 ± 1.3	0.8 ± 0.4**	–
Integrin-β3	10	4.4 ± 1.6	0.8 ± 0.6*	–
Paxillin	12	4.0 ± 1.5	0.6 ± 0.3*	–
Talin	10	5.4 ± 1.2	0.9 ± 0.5**	–
Zyxin	11	5.0 ± 1.2	0.6 ± 0.4**	–
Vinculin	12	4.7 ± 1.4	0.6 ± 0.4*	–
Paxillin + hypo-OS	5	5.0 ± 1.3	1.1 ± 0.5*	0.5 ± 0.3
Paxillin + BBI	5	3.7 ± 1.6	0.9 ± 0.6*	–
Paxillin + BBI + hypo-OS	5	3.5 ± 1.9	0.6 ± 0.3*	0.4 ± 0.3

Statistical analyses (*t* tests) were performed comparing D values in both P1 and P2 for each adhesion marker. *, P < 0.05; **, P < 0.01.

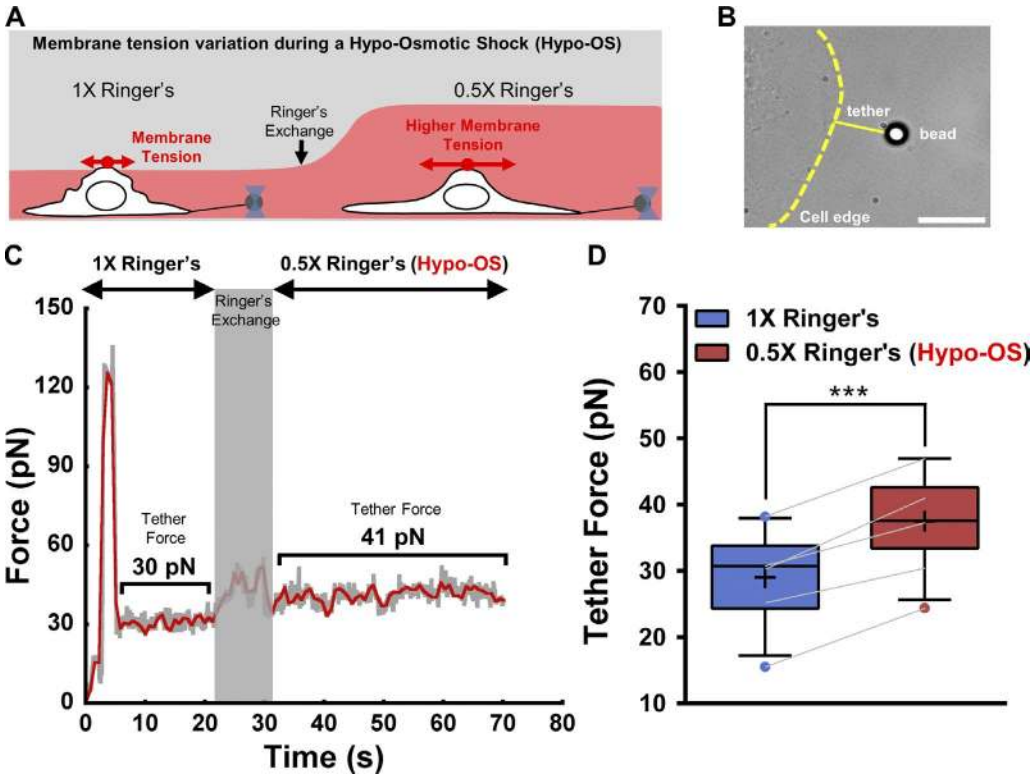

Figure 2. **Hypo-osmotic perturbation induces an increase in membrane tension.** (A) Schematic of tether extraction experiment during a hypo-osmotic perturbation. Arrows and curve, membrane tension. (B) Representative bright-field image of a tether extraction experiment. Bar, 10 µm. (C) Representative tether extraction force curve, with tether forces for 1× and 0.5× Ringer's indicated. (D) Plot of tether force values for fibroblast cells in 1× (blue box) and 0.5× (red box) Ringer's. ***, $P < 0.001$, *t* test statistics. Blue and red boxes extend from the 25th to 75th percentiles, with a black line at the median and a black cross at the mean; black whiskers extend from 5th to 95th percentiles for both conditions; values outside these ranges are plotted as individual points. Five different paired measurements, among 25 pairs of 1×/0.5× Ringer's, were chosen to represent the change in tether force observed in C. These paired measurements were correlated using a gray line in the plot.

leading edge immediately stalled, the lamellipodial actin shortened (from 3.9 ± 1.9 to 0.4 ± 0.3 µm in width), and one clear row of paxillin was positioned at the cell edge (Fig. 3, K–M; Video 3; and Table 1). When tension was restored, the cell resumed spreading (Fig. 3, K and L; and Video 3). Interestingly, the cells were also able to keep the memory of the adhesion rows that were positioned during the hypotonically elevated membrane tension (Fig. 3, L and N), but the rows never matured into large focal adhesions, in contrast to the rings of large focal adhesions in cells without BBI (Fig. 3 N compared with Fig. 3 G).

Apart from hypotonic treatments, membrane tension was also reported to increase during cell stretching (Diz-Muñoz et al., 2016). Moreover, it was proposed that cell stretching provides a clear alternative to osmotic shocks for the study of membrane dynamics (Kosmalska et al., 2015). Thus, we next decided to seed cells on fibronectin-coated polydimethylsiloxane (PDMS) substrates and perform an 8% radial stretch (Fig. 4 A, schematic). We first followed the temporal behaviors of membrane and actin in cells previously spread in a PDMS substrate before, during, and after stretch. Before stretch, the cell presented several lamellipodia (Fig. 4 B, arrow; and Video 4). During stretch, the lamellipodia collapsed and the cell edge was converted into arc-shaped structures (Fig. 4 B, arrowheads). When the stretch was released, the lamellipodium resumed (Fig. 4 B, asterisks). We next followed the temporal behaviors of actin and paxillin during stretching (Fig. 4 C and Video 4). Before stretch, a large lamellipodium was observed that contained actin and was enriched in paxillin (Fig. 4 C, arrow). Paxillin was also present in large focal adhesions at the back of the lamellipodium (Fig. 4 C, crosses). Again, during stretch, the lamellipodium was converted into arc-shaped structures, and the actin-paxillin filling the lamellipodial region disappeared (Fig. 4 C, arrowheads). Paxillin-rich focal adhesions at the back, however, were still present (Fig. 4 C, crosses). Upon relaxation, actin-paxillin–enriched lamellipodia resumed from the stretched adhesion sites (Fig. 4 C, asterisks). Myosin inhibition clearly affected actin organization and adhesion maturation, with a lack of stress fibers and focal adhesions (Fig. 4 D and Video 4). However, the cell capacity to regrow an actin-paxillin–enriched lamellipodium upon relaxation was kept intact (Fig. 4 D, asterisks). These results show that membrane stretching-relaxation is able to control lamellipodial behavior. Moreover, they demonstrate that the membrane clearly has the strength to control actin behavior independently of myosin II. Finally, the capacity to form adhesions containing paxillin is also dependent on the presence of this membrane tension–controlled lamellipodium, in a myosin II–independent manner.

We seeded cells on 8% prestretched PDMS substrates and followed their behavior after substrate relaxation. We first tracked the spatiotemporal changes in membrane and actin. Before relaxation, the cell presented several lamellipodia (Fig. 4 E, arrow; and Video 4). Immediately after relaxation, these lamellipodia first detached and lifted, forming ruffles (Fig. 4 E, arrowheads), but a new protrusion subsequently resumed (Fig. 4 E,

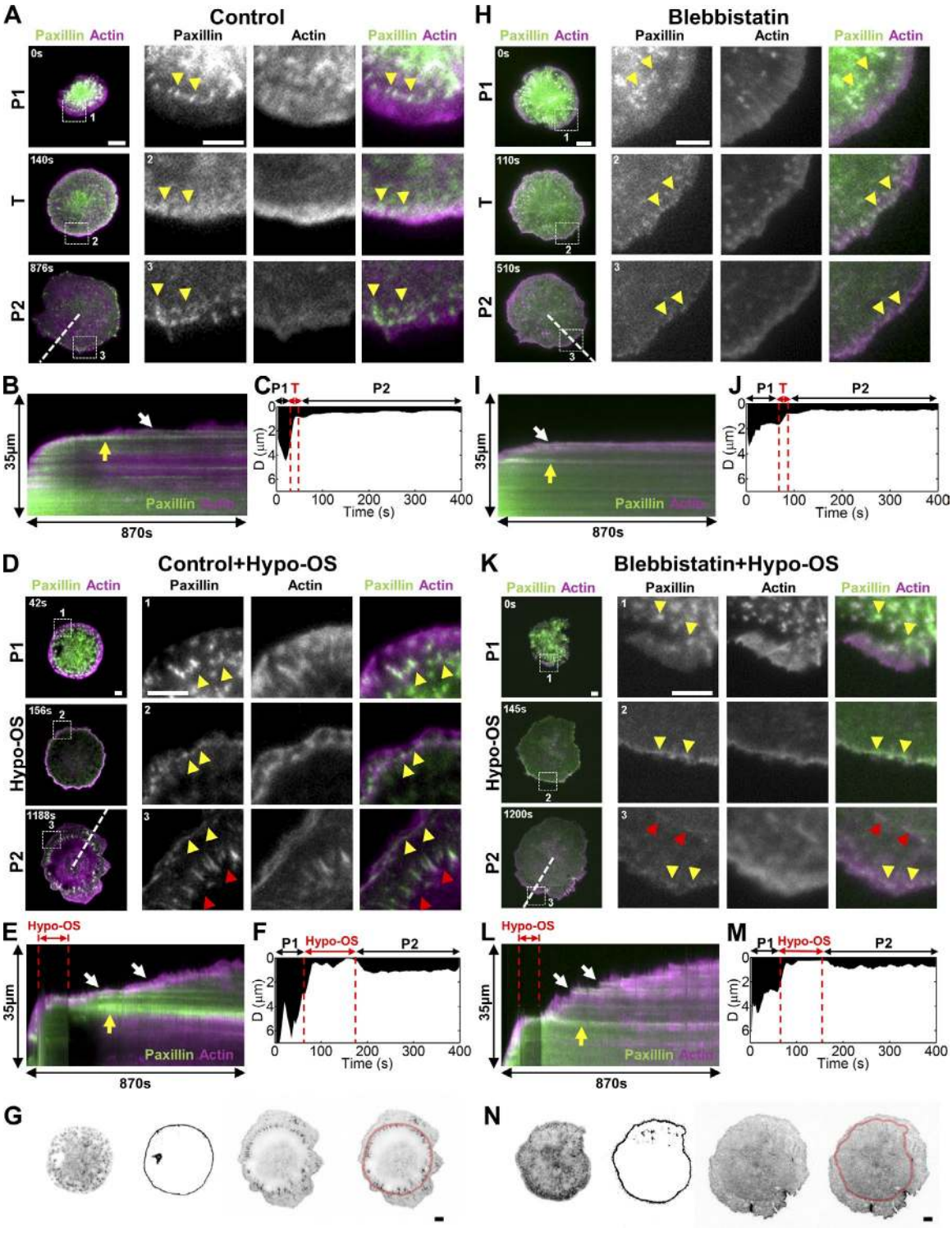

Figure 3. **Membrane tension increase induces adhesion row positioning.** Paxillin and actin behaviors followed in four conditions: control (A–C), hypo-OS (D–G), 10 µM BBI (H–J), and 10 µM BBI plus hypo-OS (K–N). (A, H, D, and K) Representative images in P1, T, or hypo-OS and P2 for actin and paxillin in all four conditions. Arrowheads, paxillin-containing adhesion clusters. (B, I, E, and L) Merged kymographs of paxillin (green) and actin (magenta) plotted from the dashed lines in A, D, H, and K. Yellow arrows, strips of paxillin-containing adhesions positioned during T (B and I) and hypo-OS (E and L); white arrows, strips of paxillin-containing adhesions positioned in P2 (after T or hypo-OS). (C, J, F, and M) Variations of D (in micrometers) during spreading for each experimental condition. Red dashed lines, beginning and end of T or hypo-OS. (G and N) Adhesion row positioned during hypo-OS (increase in membrane tension) matures into focal adhesions later in P2 in control case G but not in myosin II–inhibited cells in N, as indicated by the red outline (representing the adhesion row positioned during hypo-OS) superimposed with an image of the cell in late P2. All procedures were repeated for five different spreading cells of each experimental condition. All cells showed behaviors similar to those represented. Bars, 10 µm.

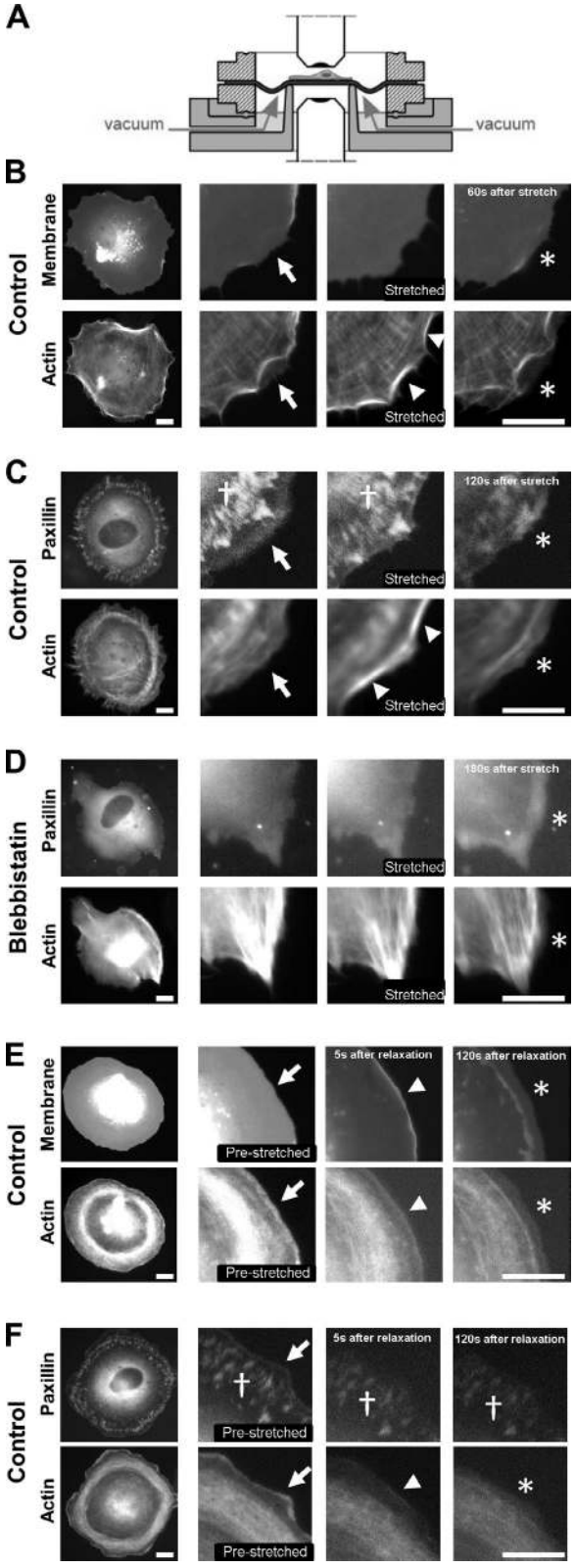

Figure 4. **Membrane tension increase by cell stretching.** (A) Schematic representation of the experimental setup used to stretch the cells. (B) Membrane and actin during cell stretching. Arrows, lamellipodial protrusion before stretch; arrowheads, collapse of the lamellipodial protrusion during stretch and formation of arc-shape structures at the cell edge; asterisks, lamellipodium reappearance when stretch is released. (C) Actin and paxillin during cell stretching. Arrows, lamellipodial protrusion before stretch; cross, paxillin focal adhesions at the back of the lamellipodium; asterisks) with widths larger than the ones present before relaxation. We also followed the behaviors of actin and paxillin during relaxation of prestretched PDMS substrates (Fig. 4 F and Video 4). Before relaxation, the cell presented several lamellipodial regions that contained actin and were enriched in paxillin (Fig. 4 F, arrow). Paxillin was also present in large focal adhesions at the back of these lamellipodia (Fig. 4 F, crosses). Again, immediately after relaxation, these lamellipodia first detached and lifted, forming ruffles (Fig. 4 F, arrowheads), but a new protrusion subsequently resumed (Fig. 4 F, asterisks), again with widths larger than the first ones. Paxillin-rich focal adhesions at the back, however, were still present (Fig. 4 F, crosses).

In summary, the different ways to increase or decrease membrane tension (osmotic treatment or cell stretching/relaxation) show that tension can control lamellipodia behavior and, as such, acts as an upstream effector on actin dynamics and adhesion positioning.

Behavior of other cytoskeletal proteins is spatiotemporally correlated with an increase in membrane tension during the P1/P2 transition of cell spreading

Apart from actin and adhesions, the behaviors of other known proteins involved in lamellipodia formation were also followed during spreading. As previously noted, VASP was present both in adhesions and at the leading edge of cells (Fig. 1 B). During P1, a line of VASP was also observed at the tip of the edges of cells (Figs. 1 B and S1 A, white arrows), a feature previously linked to the actin-polymerizing ability of this protein (Rottner et al., 1999; Bear and Gertler, 2009). When the spreading cells reached T, their VASP lines disappeared, correlating with the increase in membrane tension and decrease in lamellipodial width D (Video 1). Moreover, when membrane tension was artificially increased with a hypotonic solution, these VASP lines also disappeared, simulating what happened during T (Fig. S1 A). When tension was restored with an isotonic solution, the cells resumed spreading and VASP lines reappeared (Fig. S1 A, arrows). These results demonstrate that the VASP line at the leading edge is responding to membrane tension changes.

Arp 2/3 is an important seven-subunit protein complex known to nucleate and branch lamellipodial actin filaments (Mullins et al., 1998; Svitkina and Borisy, 1999). Cofilin is a member of the ADF/cofilin family of proteins known to sever and increase the off-rate for actin monomers from the pointed end (McGough et al., 1997). The behaviors of both Arp 2/3 and cofilin were imaged together with actin. The results showed that both Arp 2/3 and cofilin followed actin dynamics during

arrowheads, collapse of the lamellipodial protrusion during stretch and formation of arc-shape structures at the cell edge; asterisks, lamellipodium reappearance when stretch is released. (D) Actin and paxillin during cell stretching in a BBI-treated cell. Asterisks, lamellipodium reappearance when stretch is released. (E) Membrane and actin during relaxation of prestretched PDMS substrate. Arrows, lamellipodial protrusion before relaxation; arrowheads, ruffling of the lamellipodial protrusion immediately after relaxation; asterisks, lamellipodium reappearance after relaxation. (F) Actin and paxillin during relaxation of prestretched PDMS substrate. Arrows, lamellipodial protrusion before relaxation; cross, paxillin focal adhesions at the back of the lamellipodium; arrowheads, ruffling of the lamellipodial protrusion immediately after relaxation; asterisks, lamellipodium reappearance after relaxation. All procedures were repeated for at least five different cells in each condition, and all showed behaviors similar to those represented in the figure. Bars, 10 µm.

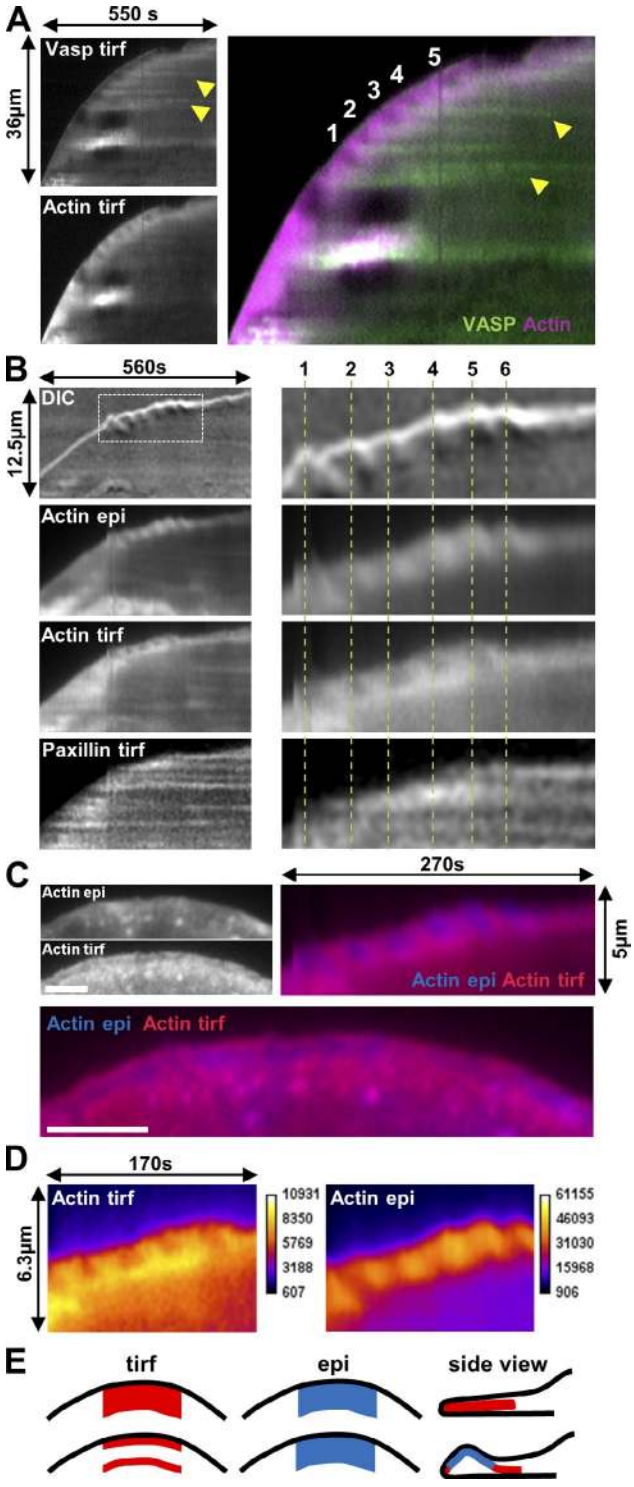

Figure 5. **Cycles of actin buckling are correlated with adhesion positioning.** (A) Tirf kymographs for VASP, actin, and their merge during five buckling cycles in P2. Arrowheads, adhesion rows. (B) DIC, epi (actin), and tirf (actin and paxillin) kymographs of a cell in P2 showing six buckling cycles. Dashed lines in zooms separate each buckling cycle. (C) Actin epi, actin tirf, and their merge showing the actin buckling at the leading edge of a spreading cell during P2. Top right color image is the same kymograph as in B, with actin epi (blue) and actin tirf (red). (D) Fluorescence intensity heat map of actin in tirf and epi for the same kymograph as in B. Fluorescence intensity levels (a.u.) are indicated as color bars. (E) Schematic top and side representations of actin buckling during P2, observed with tirf (red) and epi (blue). The experiment was repeated for 10 different spreading cells, and all show behaviors similar to those represented in the figure. Bar, 5 µm.

spreading (Fig. S1, B and C; and Video 5). Because cofilin and Arp 2/3 work together to reorganize the lamellipodial actin (Ichetovkin et al., 2002), the results demonstrate that other known actin-binding proteins respond similarly to the lamellipodium shortening in width that happens during T, when membrane tension is known to increase.

Rac1 is a member of the Rho family of GTPases. Activated Rac1 can induce cortactin to localize to the cell membrane, where it binds to actin and to the Arp2/3 complex (Weed et al., 2000). Rac1 activation then leads to the formation of a lamellipodial protrusion. We next investigated the behavior of the activated Rac1 protein during fibroblast spreading. The results showed that Rac1 activity reporter fluorescent marker (PAK-binding domain [PBD]) was intensely presented in both tirf and epifluorescence (epi) of a spreading cell during P1 but quickly dropped when this cell reached T, when membrane tension increases and the lamellipodial width decreases (Fig. S2 A). Artificially simulating the increase in tension with a hypotonic solution also led to a quick drop in fluorescence intensity for this marker (Fig. S2 B). The results demonstrate that Rac1 activity is responding to membrane tension changes.

Collectively, the results confirm that cytoskeletal proteins known as important regulators of lamellipodia organization change their dynamics during spreading in response to an increase in membrane tension. Changes in activated Rac1 are directly correlated with an increase in tension, whereas changes in Arp2/3 and cofilin are directly correlated with changes in lamellipodial actin, and actin is directly responding to changes in tension. Changes in VASP lines at the leading edge of cells could be directly correlated with an increase in tension, as VASP is linked to the plasma membrane, or with changes in lamellipodial actin, because VASP is also an actin-binding protein, as are Arp 2/3 and cofilin.

Cycles of membrane tension changes correlate with adhesion row positioning during further spreading as well as during cell migration

The membrane tension–mediated transition, T, is the first event in which a stop is observed in the lamellipodial protrusion (Gauthier et al., 2011). The spreading cell then enters P2, showing oscillating cycles of lamellipodial protrusions and brief retractions (Giannone et al., 2004, 2007). As mentioned in the Introduction, these oscillating cycles have also been reported to be key features for migration in numerous cell types (Giannone et al., 2004, 2007; Machacek et al., 2009; Burnette et al., 2011; Doyle et al., 2012).

Importantly, each of these cycles is associated with an adhesion row that is positioned at the tip of the lamellipodium (Giannone et al., 2004, 2007). Moreover, during each cycle, the lamellipodium was described to potentially bend upward, but this bending was attributed to the myosin II–mediated contractility between the new adhesion row positioned at the tip of the protruding lamellipodium and an older adhesion row previously positioned at its back (Giannone et al., 2007). We have described in this study (Figs. 1 and 3) that the increase in membrane tension observed during T is able to position an adhesion row at the leading edge of cells. It is already known that T is the first event in which cells stop their protrusions (Gauthier et al., 2011), and further stops (P2 oscillating cycles) are similar to the one in T (Gauthier et al., 2011). Thus we next asked whether

membrane tension, instead of myosin II–mediated contractility, could be able to control the bending capacity of the edge and the positioning of adhesions.

First, however, we examined the behaviors of actin and VASP during P2 spreading, with time-lapse tirf microscopy. The idea was to confirm the cyclic and oscillatory behavior previously documented (Giannone et al., 2004, 2007). We confirmed that rows of adhesions were positioned during each oscillating cycle (Fig. 5 A). Moreover, a dark region appeared in the actin tirf kymograph during each cycle (Fig. 5 A). We next performed correlative microscopies with simultaneous acquisitions of actin by tirf and epi. In addition, paxillin adhesions were imaged by tirf, and global edge behaviors were imaged by differential interference contrast (DIC) microscopy. A representative cell was chosen among several that showed similar behaviors (Fig. 5 B and Video 6). The actin fluorescence disappeared from the tirf region in all buckling cycles (Fig. 5 B), in correlation with the appearance of each DIC wave. Paxillin-containing adhesions were positioned in rows at each cycle (Fig. 5 B), similar to the observations for VASP (Fig. 5 A). Remarkably, the region that lacked actin tirf fluorescence during each period showed an increase in actin epi intensity, as seen by merging epi and tirf images (Fig. 5 C). In other words, actin disappearance from the tirf layer was correlated with elevated actin fluorescence in higher layers (epi) of the same position (Fig. 5 D). The P2 buckling cycles were also observed in cells treated with 10 µM BBI (Fig. S3, A–C). Cofilin and Arp 2/3 were followed during some oscillating cycles of edge buckling (Fig. S1, D–G), and the behavior of both resembled actin behavior during each buckling event.

Because we used a fibronectin-based spreading substrate and it is known that the primary cell receptor for this extracellular matrix protein is integrin α5β1 (Nagae et al., 2012), we next asked what the spatial distribution is of the activated integrin β1 during cell spreading and whether this activated integrin β1 is positioned at the extreme tip of a lamellipodium during an edge buckling event. During P1, activated β1-integrins (stained with the 9EG7 antibody) were in a staggered distribution along the lamellipodium (Fig. S3 D). During T or immediately after hypo-OS, activated β1-integrins were positioned at the extreme edge of the cell (Fig. S3 D), and during lamellipodia edge bucklings in P2, activated β1-integrins were also positioned in rows, one at the tip of the leading edge and another at the back of the buckling (Fig. S3 D). This result reinforces the universal adhesion behavior during an edge buckling event.

To reinforce our observations of spreading, we also followed the behaviors of actin (epi and tirf) and paxillin (tirf) during leading-edge advancements of typical migrating cells. A representative cell was chosen among several others that showed typical migratory behaviors (Fig. S4). When the migrating cell protrudes, its lamellipodium buckles upward, as can be seen by the disappearance of actin fluorescence from the tirf region but its maintenance in the epi region (Fig. S4 A). Each buckling cycle is also able to position a row of adhesions (Fig. S4 B) that is then kept in memory by the cell (Fig. S4 B). The experiment can be resumed in a kymograph that shows actin buckling and adhesion row positioning at each buckling cycle also presented in migrating cells (Fig. S4 C). These results are very similar to those observed during T and P2 spreading.

Altogether, the observed results demonstrate that a compressive force seems to cause condensation and upward buckling of the lamellipodium. A schematic representation summarizes

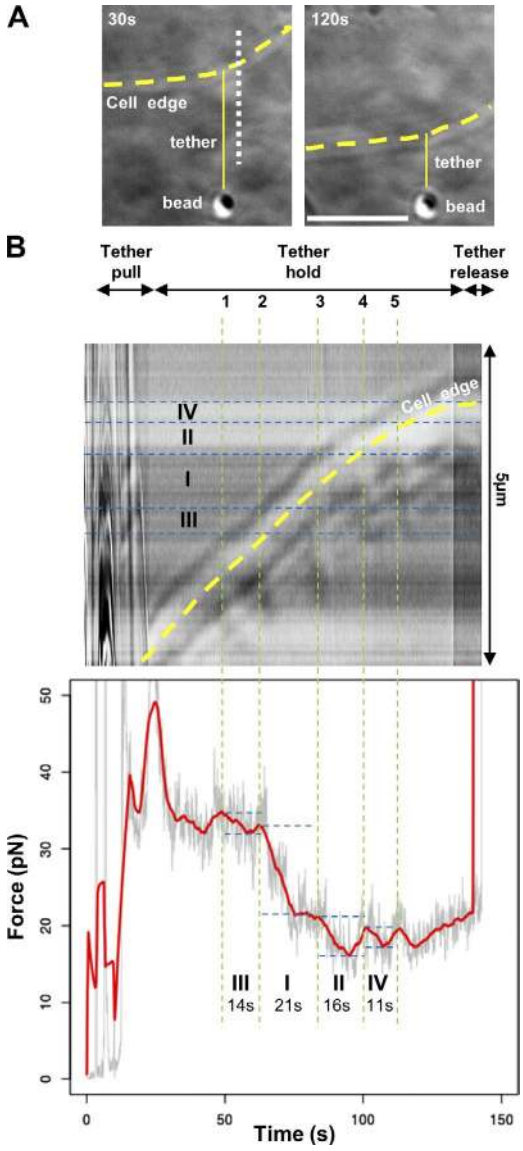

Figure 6. **Membrane tether extraction experiment during P2.** (A) Representative images of a membrane tether extraction. Yellow dashed lines, cell edge; white dashed line, region where the kymograph presented in B was generated. Bar, 5 µm. (B) Correlation between cell edge motion (kymograph) and tether force during four bucking cycles (I, II, III, and IV). Green dashed lines separate the buckling events as a function of edge position; blue dashed lines determine edge extension (in the kymograph) or variations in tension (in the curve) for each buckling event; plot in red, 2-s moving mean.

the experiment, showing the regions that were observed with each mode of imaging (Fig. 5 E).

We then investigated whether this compressive force, which is able to cause cell edge stall and lamellipodial buckling with adhesion row positioning, would originate from a temporary increase in membrane tension. Such an association could indicate a role for membrane tension not only during T, but also during P2 and other edge oscillations observed during cell migration. To monitor the changes in membrane tension, membrane tethers were extracted from the lamellipodia of spreading cells using optical tweezers (Dai and Sheetz, 1999; Gauthier et al., 2009, 2011; Pontes et al., 2011; Houk et al., 2012). A membrane tether was extracted and maintained intact

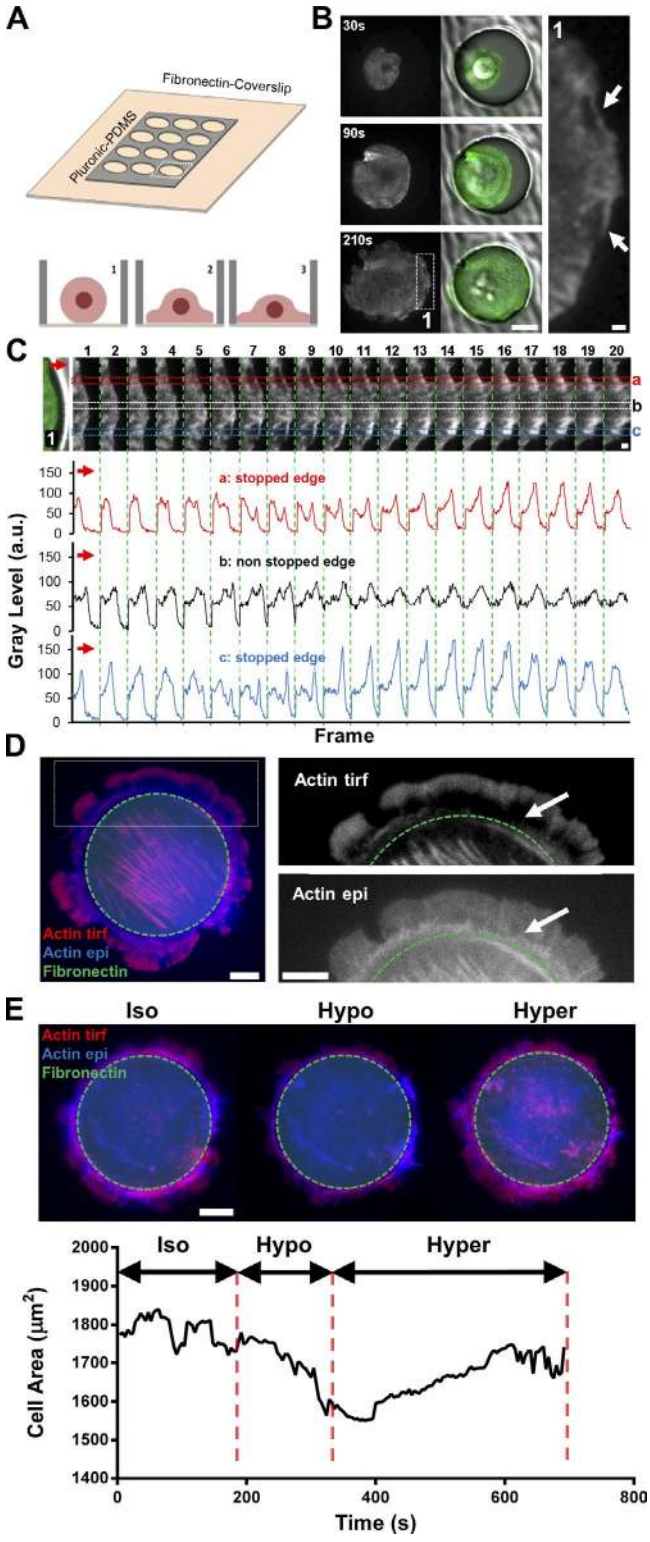

Figure 7. **Mechanically mimicking the membrane tension load induces lamellipodial actin buckling.** (A) Schematic representation of the experiment. (B) Representative cell spreading inside a well. Actin in tirf (left), actin merged with DIC (middle), and zoom at the moment actin encounters the barrier. Arrows, two actin buckling events. (C) Time-lapse analysis of the actin buckling for stopped edge (a [red] and c [blue]) or unstopped edge (b [dark]). Graphs represent the intensity profiles of the selected a, b, and c regions of each frame (1–20) of the panel on top of the graphs. Green dashed lines are guides to determine the limit of each frame. (D) Representative frame and zooms showing actin fluorescence (tirf in red and epi in blue) of a cell attached to a 45-µm-diameter fibronectin circle (green). Arrow, buckled actin. (E) Representative frames showing actin fluorescence (tirf in red and epi in blue) of a cell attached to a 40-µm-diameter fibronectin circle (green) during iso-, hypo-, and hypertonic exchanges. Plot represents the variation in the overall cell area (square micrometers) of actin epi during each of the media exchanges. Dashed lines are guides to determine each medium exchange. Bars: (B, D, and E) 10 µm; (B [zoom 1] and C) 1 µm.

for ∼150 s in a representative cell at the beginning of the P2 spreading phase (Fig. 6 A and Video 7). This experiment allowed us to follow the membrane tension dynamics during P2. The membrane tension decreased between the start and the end of the experiment (Fig. 6 B). This is in agreement with previous results showing an overall decrease in membrane tension from T to later in P2 (Gauthier et al., 2009). However, the decrease was nonmonotonic, and four cycles of increase–decrease were observed (labeled I–IV in Fig. 6 B) with a mean period of 16 ± 3 s. These cycles of membrane tension variations were in phase with the cycles of edge stall and buckling, whereby peaks in tension were correlated with stalled edges and lamellipodia bucklings and decreases in tension were associated with protrusion restorations (Fig. 6 B). Moreover, the displacement and duration of cell edge protrusion during each cycle was correlated with the extent of membrane tension change. Longer protrusion lengths were associated with larger drops in membrane tension (Fig. 6 B, I and II), and shorter protrusion lengths were associated with smaller drops in tension (Fig. 6 B, III and IV). Also, the edge protruded more rapidly in cycles that showed smaller increases in membrane tension (Fig. 6 B, I, III, II, and IV). Finally, the longer the decrease-increase cycle of tension, the longer the time between the formation of each DIC wave (I to IV, longest to shortest; I, 21 s; II, 16.5 s; III, 14 s; IV, 12 s).

In summary, the results show that during typical oscillatory cycles, observed in spreading and migratory cells, the cell edge stalls and the lamellipodium buckles upward, positioning rows of adhesions exactly when the membrane tension temporary increases. When tension decreases, the protrusion resumes and buckling disappears, until the next cycle.

Mechanically mimicking membrane tension load induces lamellipodial actin buckling

Based on our observation that the lamellipodial actin buckles upward because of the increase in membrane tension, we next hypothesized that a lateral compression of lamellipodial actin would reproduce the buckling event. To test this hypothesis, artificial barriers were designed to confront protruding lamellipodia during normal cell spreadings. Cylindrical PDMS wells were prepared and placed on top of fibronectin-coated coverslips. Cells were seeded inside the wells and allowed to spread (Fig. 7, A and B; and Video 8, top). The entire cell behavior was recorded with DIC, and lamellipodial actin behavior was recorded with tirf. As expected, when the leading edge of a cell collided with the wall, the spreading halted and the lamellipodial actin buckled (Fig. 7 B and Video 8, top). A more careful analysis of the actin intensity profile showed two narrow regions of tirf fluorescence, one at the cell edge and another located about a micrometer inward (Fig. 7 C). The buckling observed when confronting obstacles (0.9 ± 0.4 µm in width) resembled the buckling observed during P2 (Fig. 5; i.e., non-myosin–based buckling). The buckling lasted for ∼20 s, a period quite similar to those previously reported in normal P2 cycles, demonstrated

in this study and Giannone et al. (2007). After buckling, the region lacking tirf fluorescence consistently regrew from the edge inward, suggesting that actin was polymerizing inward along the ventral surface (Fig. 7 C and Video 8, top). Because the PDMS forming the well was somehow imperfect and presented wave-like patterns, it allowed certain regions of the lamellipodium to continue to spread under the well, providing convenient internal controls for the barrier-induced buckling (Fig. 7, B and C; and Video 8, top).

The well-based experiment demonstrated that the buckling induced by a mechanical barrier at the tip of the leading edge was similar to the buckling induced by the increase in membrane tension during P2. However, to further strengthen this similarity, another experiment was designed. This approach was intended to force the cell to have the membrane mechanical feedback at the lamellipodial tip without potential interferences from a new adhesion row, while keeping the back of the lamellipodium attached to an older adhesion row. Cells were seeded on microcontact-printed 45-µm-diameter fibronectin circles surrounded by a nonadhesive substrate. After spreading, the cell presented stress fibers and a broad isotropic lamellipodium (~5 µm in width, similar to P1 spreading phase) extending away from the fibronectin circle and over the nonadhesive region (Fig. 7 D and Video 8, middle). By simultaneously following actin with tirf and epi, clear and very broad buckling was observed (dark region observed with tirf and bright with epi) between the extreme edge of the fibronectin (green circle) and the tip of the lamellipodium. Moreover, using this same experimental setup, we simultaneously followed actin (in tirf and epi) during hypotonic and hypertonic shocks. Immediately after a hypotonic treatment, cells that were previously in isotonic media decreased the width of their lamellipodia protrusions, as can be seen by the decrease in the cell's overall fluorescence area (Fig. 7 E and Video 8, bottom). This result recapitulates what we present in this article: the hypotonic shock increases membrane tension and decreases lamellipodia protrusions. After the hypotonic treatment, a hypertonic medium was subsequently added, and restorations of lamellipodial protrusions were observed (Fig. 7 E and Video 8, bottom).

These two different approaches (PDMS wells and microcontact-printed circles) show that buckling is induced by the membrane tension load at the tip of the lamellipodium. Moreover, adhesions at the back are required to hold the lamellipodial actin to counteract the membrane tension load. We next asked what mechanism accounts for this load imposed by the membrane tension.

Vinculin controls membrane tension–dependent adhesion positioning

The link between lamellipodial actin and adhesions has been proposed to occur through a molecular clutch engaging actin and integrin through vinculin (Thievessen et al., 2013). If this is true, then in our situation, vinculin should provide the mechanical connection between the lamellipodial actin and the adhesion row to resist the membrane tension increase. To test this hypothesis, MEFs knocked out for vinculin (vinculin KO cells) were transfected with a construct that expresses a vinculin mutant containing only the head domain (unable to bind actin) and compared with vinculin KO cells that were transfected with a construct expressing the WT vinculin (capable of binding actin; Fig. 8). Nontransfected vinculin KO cells and vinculin KO cells transfected with either VASP or paxillin or stained

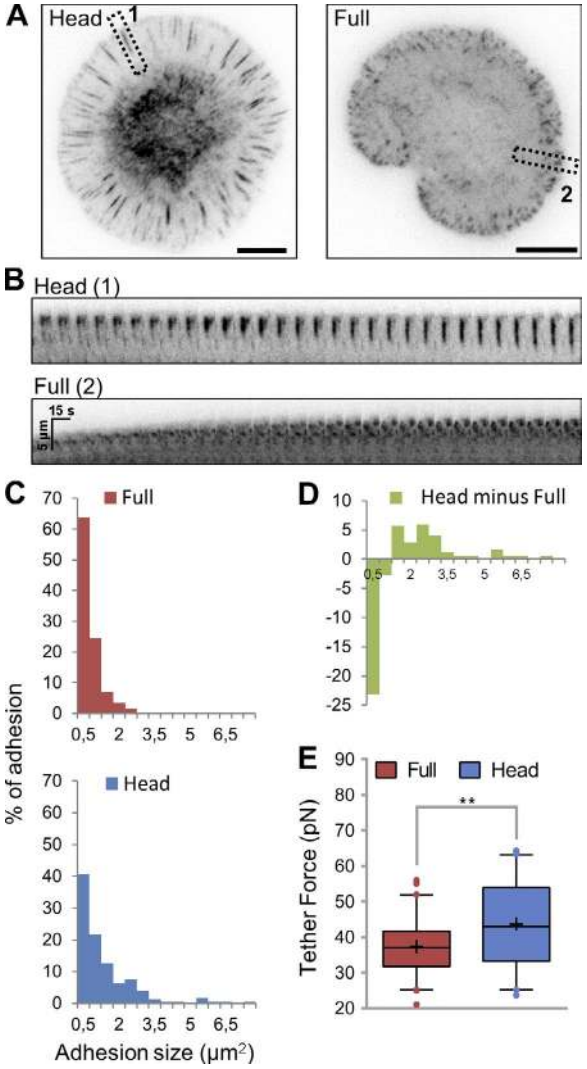

Figure 8. **Adhesion dynamics is spatiotemporally correlated with an increase in membrane tension in a vinculin-dependent manner.** (A) Representative images in late P2 of vinculin KO cells transfected with vinculin head and vinculin full. Bars, 10 µm. (B) Time-lapse images at the transition T of focal adhesions dynamics from A for vinculin head (1) and vinculin full (2). (C) Histogram of vinculin-containing adhesion sizes after 15-min spreading in vinculin full (red) and vinculin head (blue) cells. (D) Histogram of the shift in adhesion sizes from vinculin head to vinculin full. (E) Plot of the tether force values for vinculin full (red box) and vinculin head (blue box). **, $P < 0.01$ in *t* test statistics. Blue and red boxes extend from the 25th to 75th percentiles, with a black line at the median and a black cross at the mean; black whiskers extend from 5th to 95th percentiles for both conditions; values outside these ranges are plotted as individual points. The procedures in A–D were repeated for at least 15 different cells in each experimental condition. All cells showed behaviors similar to those represented in the figure. The procedures in E were repeated for at least 60 different cells of each experimental condition.

with activated β1-integrins were used as controls (Fig. S5 A). In all cases, cells were able to spread isotropically in P1, showing staggered adhesions. During T, an adhesion row was positioned at the edge of cells in all conditions. However, in P2, although the cells transfected with the full-length vinculin displayed the typical multiple adhesion rows and short lamellipodia (Fig. 8, A and B; and Video 9), the head domain–transfected cells (Fig. 8, A and B; and Video 9) and the vinculin KO cells used as controls (Fig. S5 A) displayed a very different pattern. Right after

the transition, positioned adhesions started to elongate inward. This was also associated with a very broad and dynamic lamellipodium with a strong retrograde actin flow (compared with the vinculin KO cells back-transfected with the full-length vinculin construct). Head domain cells and controls were unable to position new adhesion rows after T (Video 9). The results were confirmed by quantifying adhesion sizes after 15 min of spreading (Fig. 8 C), with the head domain–transfected cells showing a clear shift toward much larger adhesions (Fig. 8 D).

We then asked whether membrane tension is different between various tested situations (full, head, and nontransfected vinculin KO cells). If it is, then nontransfected vinculin KO cells or the ones transfected with the head domain should present higher values of membrane tension, as they cannot move forward despite strong actin polymerization. Membrane tether experiments were performed in each of the situations (Fig. S5, B and C). The mean tether forces for nontransfected and head domain–transfected cells were 43 ± 1 and 44 ± 2 pN, respectively, values quite high compared with the mean tether force of the vinculin full cells (37 ± 1 pN; Figs. 8 E and S5 D). The tether force values can be translated into a higher membrane tension in nontransfected and head domain–transfected vinculin KO cells compared with vinculin full cells (the membrane tension is proportional to the square of the tether force).

Altogether, the results were able to better define the mechanisms behind the changes in membrane tension load. The mechanical signal of membrane tension is carried and transmitted by the lamellipodium to the substrate. This transmission occurs by adhesion positioning through the vinculin–actin engagement. Moreover, when vinculin is capable of engaging in actin (vinculin full cells), membrane tension decreases and the cells can resume protrusion and form other adhesion rows. However, when vinculin is unable to engage in actin (nontransfected or head domain–transfected cells), the membrane tension remains high and cells do not show periodic cycles of protrusion-retraction with leading edge buckling.

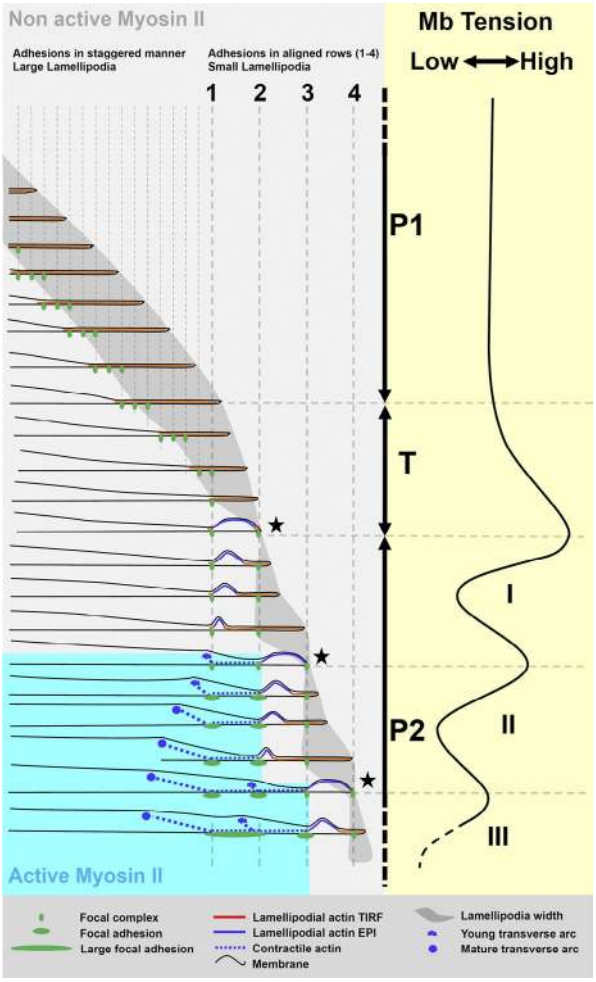

Figure 9. **Schematic representation of membrane tension-mediated adhesion positioning during spreading.** This figure is described in the Discussion.

Discussion

Membrane tension is increasingly appreciated to be a key regulator of cell functions (Keren, 2011; Gauthier et al., 2012; Nassoy and Lamaze, 2012; Diz-Muñoz et al., 2013; Sens and Plastino, 2015). Here, we found that an increase in tension exerts an upstream control in mechanotransduction by compressing the lamellipodium. Subsequently, the lamellipodium acts through vinculin to transmit the membrane tension load to adhesions. As a consequence, adhesions align in rows on the substrate. Our results show that an increase in tension is able to change the behavior of the molecules that organize cell motility at the leading edge. Moreover, the results unveil a new mechanosignaling cascade in which several elements are affected by a physical signal, originated in the plasma membrane and transmitted through the lamellipodium to adhesions on the substrate.

A new vision for adhesion positioning that integrates membrane dynamics

The discussion of our results is presented in parallel with a schematic representation that we propose in Fig. 9. As previously reported, during P1, membrane tension stays relatively constant (Gauthier et al., 2011). Our results show that a wide lamellipodium (~5 µm) protrudes at a constant speed, with actin polymerization pushing the membrane. Numerous early adhesions are staggered at the back of the lamellipodium, providing anchor points for forward movement. Almost no actin retrograde flow is observed, corroborating previous studies (Giannone et al., 2004, 2007) and indicating that the actin polymerization in P1 is entirely dedicated to push the membrane forward. This situation is probably maintained because cells present a large amount of available membrane buffers, used to increase their spreading area (Gauthier et al., 2011, 2012; Masters et al., 2013). However, as soon as these membrane sources get depleted, the cells start the transition T (Gauthier et al., 2011, 2012; Masters et al., 2013).

During T, membrane tension increases, reacting against the pressure exerted by the polymerizing actin (Gauthier et al., 2011; Lieber et al., 2013; Masters et al., 2013). Our results demonstrate that the lamellipodium gets compressed and reduces its protrusive speed. At this moment, the adhesions near the edge are reinforced, whereas the ones further back are dissipated (the distance D between adhesions and the border of the cell drops from ~5 to ~1 µm in width, regardless of the adhesion markers tracked). The reinforced adhesions are now able to carry the membrane tension load, transmitted through actin. Furthermore, corroborating our observations, this is also the moment when actin retrograde flow increases in the lamellipodium (Giannone et al., 2004, 2007).

Our results also show that the transition T can be simulated (or anticipated) during spreading by artificially increasing membrane tension, which similarly makes one single row of adhesions at the edge, in a myosin II–independent manner. To the best of our knowledge, this article is the first to show cell-based experimental proofs of this membrane tension-based regulation. However, it is worth mentioning that the 50% hypotonic shock simulates T only when performed in spreading cells in late P1. In this particular situation, spreading cells are near their membrane depletion in term of folds, but they do not show active membrane trafficking; the entire cell is only devoted to push the membrane through lamellipodial protrusion (Gauthier et al., 2011). All these features can explain why spreading cells in late P1 are sensitive to hypo-osmotic perturbations. The same 50% hypotonic treatment, however, was not able to eliminate all folds and ruffles from the MEF cell condition used by Kosmalska et al. (2015). In their experiments, the MEFs were seeded and allowed to spread for 30–60 min. This means that these cells have their membrane trafficking fully restored (exocytosis in particular), and numerous folds are again present. Thus, upon hypo-OS, some folds may disappear, but a large amount of membrane can be compensated for by slowing the endocytosis and increasing the exocytosis, as well. In the case of a fully spread cell, the cell is in a geometric constraint where just a slight change in height can accommodate the required change in volume with minimum surface area modification.

Regarding cell stretching, our results demonstrate that most cell structures (stress fibers and adhesions) are maintained after stretch. However, lamellipodial regions disappeared and are converted into arcs. How do we explain the lamellipodia disappearance, taking into account the increase in membrane tension during stretching? We believe that the stretch is being applied not only to the stress fibers and adhesions but also to lamellipodia and plasma membrane. All these structures are bearing the load imposed by the stretch. The plasma membrane reacts by immediately increasing its tension. The stress fibers and adhesions react by expanding but keeping the structure more or less intact. We believe that the lamellipodia would also increase in area during cell stretching. During this expansion, the lamellipodia would try to push the membrane, but because the membrane tension is high, the lamellipodia bear the load imposed by the membrane, immediately decreasing in size and becoming arcs at the cell edge. When the stretch is released, the membrane tension decreases, and new lamellipodia can again appear. Moreover, MEFs seeded on prestretched substrates form larger lamellipodia when the stretch is released, reaffirming that membrane relaxation contributes to protrusion restoration.

We observed that VASP, Arp 2/3, cofilin, and Rac1 behaviors all change during the transition T, when tension is known to increase. Our observations for VASP are in total agreement with a previous study demonstrating that the VASP line at the tip of the edge disappears when a cell confronts a mechanical barrier (Fig. 8 in Lacayo et al. [2007]). The membrane tension–mediated barrier seems true not only for actin and VASP, but also for other actin-binding proteins known to modulate lamellipodial protrusion. Arp 2/3 and cofilin both decrease their width in the lamellipodium during T, following actin behavior. Signaling behavior is also in agreement with Rac1 activity modulated by membrane tension, as previously demonstrated by us (Masters et al., 2013) and others (Houk et al., 2012). We observed Rac1 activity in lamellipodium and lamella regions, and although it does not follow actin dynamics during spreading, we believe that it is still driving the Arp2/3-dependent actin polymerization at the lamellipodium by activating Arp2/3 that is then moving together with actin. Activation zones do not have to match 100% with effective working zones, particularly because only a small pool of Arp2/3 may be activated in the lamella but a large pool may be active and working together with actin in the lamellipodia.

The transition T lasts ∼30 s. Simultaneously, and as previously reported, the cell responds to the increase in tension by activating exocytosis to increase its membrane area (Gauthier et al., 2011, 2012; Masters et al., 2013) and starts myosin II–mediated contractility (Giannone et al., 2004, 2007; Gauthier et al., 2011). These two events mark the end of T.

The cells then enter the P2 spreading phase. We conjecture that at this moment, the spreading cells have only two ways to decrease the membrane tension: through exocytosis (Gauthier et al., 2011) or by reducing the pressure exerted by the lamellipodial actin against the membrane through activation of myosin II–mediated contractility (Gauthier et al., 2011; Lieber et al., 2013). These two phenomena (exocytosis and contractility) may explain why we observed an overall decrease in tension from T to later in P2 (Fig. 6 B). It also explains why we and others observed some short retraction events previously reported to be associated with the pausing of the edge (5 s of the 25-s typical cycle length; Giannone et al., 2004, 2007) and also why myosin II–inhibited cells show higher membrane tension thresholds (Gauthier et al., 2011; Houk et al., 2012), although they globally spread like control cells (they show all P1, T, and P2 modifications described for control cells). More broadly, in migrating cells, membrane requirements can also be provided by the retraction of the trailing edge, or even weakening or shrinking of cell parts, as already proposed for keratocytes (Keren et al., 2008). As new membrane area becomes available, membrane tension decreases and actin polymerization at the leading edge can again push the membrane forward, resuming lamellipodial protrusion. Some actin also flows backward, probably moving above the adhesion layer or polymerizing from adhesion sites (Yu et al., 2011). Our results on the proportionality between tension drop and lamellipodial capability of extension show that the protrusion extension is linked to the cell's ability to provide new membrane area. Our results also show that the lamellipodium then grows in width and leads the way for a new increase in membrane tension. However, as the membrane tension load increases at the tip, it mechanically prompts the lamellipodial actin to buckle away from the substrate. As a consequence, the lamellipodial protrusion slows down and reaches an almost complete stop. This observation is reinforced when buckling is simulated, either when the tip of the edge is abruptly stalled (PDMS well experiment; Fig. 7, A–C) or when the lamellipodium is able to extend to its maximum width without a new adhesion row to hold the load imposed by the membrane tension (circle experiment; Fig. 7 D). Moreover, other evidence demonstrates that a mechanical load is able to make self-assembling actin networks in vitro (Risca et al., 2012; Bieling et al., 2016). We conjecture that fluctuations in mechanical load in vivo can be performed by the membrane tension. At maximum buckling, lamellipodial speed is greatly reduced while its tip remains in contact with the substrate, as shown by our results on the presence of both actin and adhesion proteins at the tirf region. This favors adhesion positioning only at the tip, leading to a new row of adhesion similar to the one previously positioned during T (Fig. 9, star). However, as more membrane continues to be provided by exocytosis, the

increased tension can now decrease, and a new lamellipodial protrusion resumes, while the buckling gets pushed backward, creating the typical wavelike structure observed in DIC. This wave structure will be later condensed, creating the myosin II–associated transverse arcs, as previously suggested (Giannone et al., 2007) and elegantly demonstrated using structured illumination microscopy (Burnette et al., 2014). Our results show that multiple buckling cycles occur and several rows of adhesion are then positioned, one at a time, at each cycle. Moreover, the edge bucklings observed in this study during P2 and lamellipodia-based 2D cell migration, which lasts ∼25 s, are not controlled by changes in fluctuations of Rac1 activity because we do not see any activated Rac1 variation during P2 buckling cycles (activated Rac1 seems to be off after T). Our hypothesis is that the edge bucklings observed by us in this study are part of an autonomous "dampening" mechanism relying only on membrane availability and actin polymerization. This is different from what was previously proposed for longer cycles of protrusion-retraction (∼2 min; Machacek et al., 2009). To the best of our knowledge, we are the first to experimentally correlate lamellipodial actin buckling and adhesion row positioning with a temporary increase–decrease in membrane tension during P2 protrusion-retraction cycles. Finally, we also observed the same phenomena in a polarized migrating cell (see Fig. S5). In summary, we are now capable of understanding how membrane tension changes induce cell edge buckling and adhesion positioning during all phases of spreading/migration.

Computational modeling confirms that membrane tension leads the way

To integrate our experimental findings about lamellipodial mechanics, we developed a bidimensional simulation of cell edge protrusion (Video 10). A complete specification of the mathematical model appears in Materials and methods. In brief, this simple model is capable of positioning adhesions near the cell edge according to two criteria: a stochastic probability that increases as the cell edge protrudes farther from the previous adhesion and a deterministic criterion that makes an adhesion whenever the membrane tension exceeds a fixed threshold. The cell edge protrusion was assumed to be driven by polymerization of an actin mesh, modulated by membrane availability. The model simulations are sufficient to recapitulate the experimental patterns observed, including stochastic positioning during P1, narrowing of the lamellipodium during T, and periodic, synchronized positioning during P2 (Video 10). In addition, simulated membrane tension increase was assumed to exert compressive force on the protruding actin. We computed a hypothetical threshold for the amount of compressive force necessary to cause buckling instability based on the span length of the actin mesh protrusion, but without other physical parameters for the actin mesh. At each time point of the simulation, an actin segment was annotated with an asterisk if its compressive load was greater than its current buckling threshold (Video 10). The buckling simulations resembled the experimental observations; in both model and experiments, buckling of the edge terminated when distal adhesions were positioned.

Actin buckling: A universal mechanism?

Because the buckling issues we address are potentially applicable to many contexts, we sought supporting evidence in existing datasets from other cell types. Keratocyte migration has been imaged using interference reflection microscopy, which identifies differences in height of distinct regions of an object in contact with a glass surface (Oliver et al., 1999; Gabella et al., 2014). Interestingly, when keratocytes were plated on a glass coverslip, the lamellipodia displayed a thin line at the tip of the edge in close contact with the substrate, separated from a large region at the back by a gap of ∼1–2 µm (higher region relative to the glass substrate; Fig. 11 a in Oliver et al. [1999] and Fig. 3 D in Gabella et al. [2014]). This gap is not mentioned in the articles, but the phenomenon could be analogous to the buckling observed in our fibroblast cell system. Furthermore, as already shown, keratocytes use membrane tension to keep their shape, whereas myosin II localizes at the rear of these cells, far from the leading edge (Keren et al., 2008; Keren, 2011; Lieber et al., 2013), indicating that the potential buckling is not directly linked to myosin II activity but probably through membrane tension control. Considerable other evidence shows protrusion rates to be strongly and inversely correlated with increases in membrane tension (Raucher and Sheetz, 2000; Kozlov and Mogilner, 2007; Keren et al., 2008; Gauthier et al., 2011; Houk et al., 2012; Lieber et al., 2013; Masters et al., 2013; Schweitzer et al., 2014). However, Batchelder et al. (2011) showed that membrane tension is positively correlated with protrusion rate, but their *Caenorhabditis elegans* sperm cell system is biochemically distinct from the actin-based motility that we are studying, and we do not claim that the two systems are analogous. In summary, evidence observed in keratocytes supports the mechanisms inferred for fibroblasts, suggesting that similar underlying mechanisms may be relevant for multiple other vertebrate cell types.

The membrane–actin–vinculin mechanical chain

In this study, we link membrane tension with adhesion positioning, and we propose that the membrane tension signal is transmitted to adhesions through compression of lamellipodial actin and through the actin-binding domain of vinculin. Vinculin bridges actin and adhesions (Carisey et al., 2013; Dumbauld et al., 2013; Thievessen et al., 2013) and works to transmit force as part of a molecular clutch complex composed of fibronectin, integrin, talin, and actin (Thievessen et al., 2013; Case et al., 2015). In our spreading system, vinculin is enriched at adhesions after the increase in membrane tension. When we deleted vinculin's actin-binding domain, the lamellipodial actin retrograde flow increased enormously, indicating that vinculin-actin binding is necessary for mechanical engagement between lamellipodial actin and adhesions. Moreover, the membrane tension values in these cells remained high after T. In addition, deletion of the actin-binding domain caused adhesions to grow very large. We believe that the adhesions continue to grow because they fail to engage in actin filaments. This interpretation arises from the work of Thievessen et al. (2013), which provided an elegant demonstration that the size of vinculin focal adhesions has no correlation with the force exerted against the substrate.

Lamellipodial buckling also seems to be directly linked to the boundary conditions at its rear. For the buckling to occur, not only does membrane tension need to increase but the adhesions positioned at the back of the lamellipodium also need to be well attached to the substrate and clutched to the lamellipodial actin cytoskeleton. If a cell is in this situation, its lamellipodium bends upward and transmits the membrane tension load to the adhesions at the back. This is what happens in the normal MEF and the vinculin KO cells transfected with the vinculin full-length construct. However, in nontransfected vinculin KO cells or vinculin KO

cells transfected only with the vinculin head domain construct, the membrane tension load is not transmitted through the lamellipodial actin to the positioned adhesions because they are not well engaged (lack of proper vinculin domain that engages with actin). Thus, no buckling occurs, the membrane tension remains high if there is a lamellipodium pushing the membrane, and the load is not transmitted to the adhesions, because there is no clutch between the lamellipodial actin and adhesions. Adhesions are not always perfectly aligned along all regions of the lamellipodium, however; some regions are aligned and engaged with the lamellipodial actin to sustain the membrane tension load. In these regions, the lamellipodium is able to buckle upward. But in lamellipodial regions where adhesions are not well aligned or clutched to actin, the buckling also does not occur.

Membrane tension is key for adhesion positioning

Based on previous published data using the same cell type (MEF; Gauthier et al., 2011; Meacci et al., 2016), we can estimate the force needed for nascent adhesion positioning. In Gauthier et al. (2011), it was found that during the P1/P2 transition, the tether force increased to ∼37 pN. This tether force is related to a membrane tension of the order of 10^{-4} N/m, which is able to induce a loading force of around 1 nN/μm^2 against the leading edge. Because the lamellipodium is ∼100 nm in height and is reduced to ∼1 μm in width during the P1/P2 transition, the force exerted by the membrane tension against the lamellipodium is ∼100 pN/μm of edge. This could be the force that adhesions in the edge encounter to stabilize. The number of adhesions is hard to estimate from our fluorescence microscopy results, however, and we propose that a 1-μm line of adhesions parallel to the edge will have to carry this 100 pN. The 37 pN of tether force estimated (Gauthier et al., 2011) is compatible with the force presented in this article (∼35 pN during T to ∼17 pN in late P2 at 120 s; Fig. 5 B). Using cells that spread over pillars, Meacci et al. (2016) showed that, during a protrusion retraction cycle, pillars closer to the cell edge displace inward, whereas pillars located 2 μm behind displace outward. The inward displacements were of the order of 60 nm, and the outward displacements were 35 nm. Thus, the difference between them was 25 nm inward, which gives a difference in inward force on the order of 350 pN per pillar (pillar bending stiffness, 13.9 pN/nm). The spacing between the hexagonal pillar arrays was 1 μm, so each pillar could then be considered as one adhesion point and has to carry 350 pN of force (see Fig. 1 in Meacci et al. [2016]), a value quite compatible with those found after membrane tension estimations (described to be ∼100 pN/μm of edge).

In conclusion, we propose that the mechanical signal of membrane tension can act as a key parameter organizing the cell's leading edge, constraining actin protrusions, buckling the lamellipodia, and orchestrating molecular machineries to trigger adhesion row positioning during cell migration.

Materials and methods

Cell culture, reagents, and transfections

Immortalized normal MEFs and vinculin KO MEFs were cultured in DMEM with 10% FBS at 37°C and 5% CO_2. All culture reagents were obtained from Gibco. Transient transfections were performed the day before the experiment using the Neon electroporation system (Thermo Fisher Scientific). Plasmids used in this study were Arp3-mCherry (27682; Addgene; deposited by C. Merrifield, Institute de Biologie Intégrative de la Cellule, Centre National de la Recherche Scientifique, Gif-sur-Yvette, France), PBD-Ypet (22781; Addgene; deposited by K. Hahn, University of North Carolina, Chapel Hill, NC), zyxin-RFP (26720; Addgene; deposited by A. Huttenlocher, University of Wisconsin-Madison, Madison, WI), cofilin-mCherry (27687; Addgene; deposited by C. Merrifield), integrin β3–GFP (Plançon et al., 2001), VASP-GFP (Giannone et al., 2007), talin-RFP (Zhang et al., 2008), paxillin-mCherry (gift from C. Waterman, National Institutes of Health, Bethesda, MD), vinculin-mCherry and vinculin_head-mCherry (gifts from P. Kanchanawong, Mechanobiology Institute, National University of Singapore, Singapore), actin-GFP and actin-RFP (gifts from E. Lemichez, Centre Méditerrenéen de Médecine Moléculaire, INS ERM, Nice, France) and membrane-GFP (Takara Bio Inc.). Immunofluorescences were performed using a BD rat anti-mouse CD29, clone 9EG7, and costained with actin using phalloidin-FITC (Sigma-Aldrich). In brief, cells were fixed in PBS and 4% PFA for 15 min, permeabilized with PBS and 0.2% Triton X-100 for 5 min, blocked with PBS and 5% BSA for 1 h, incubated with 9EG7 antibody for 1 h, and incubated with the secondary antibody and phalloidin for 1 h.

Spreading assays

MEFs were trypsinized and suspended in 1× Ringer's solution (150 mM NaCl, 5 mM KCl, 1 mM $CaCl_2$, 1 mM $MgCl_2$, 20 mM Hepes, and 2 g/liter glucose, pH 7.4) for 30 min before spreading assays. The coverslips were previously acid-washed with a 20% solution of HNO_3 and coated with 10 μg/ml fibronectin for 2 h at 37°C. The coverslips were then mounted in chambers and transferred to the microscope, where cells were allowed to spread. A 10-μM BBI (Sigma-Aldrich) solution was used to inhibit myosin II–mediated contractility. BBI-treated cells were incubated for 30 min before spreading. For hypo-OS, a hypotonic exchange (0.5× Ringer's) followed by a restoration of isotonicity (1× Ringer's) was performed. For hypo-OS experiments with BBI-treated cells, a 10-μM concentration of BBI was present in both hypotonic and isotonic media, to maintain the drug concentration throughout the experiment. 1.5× Ringer's was used as hypertonic medium. All spreading assays were performed at 37°C.

Microscopy

DIC, tirf, and epi time-lapse microscopy of spreading cells were performed using an iLas^2 targeted laser illuminator system (Roper Technologies) adapted to an IX 81 microscope (Olympus). Images were acquired using either a PlanApoN 60× 1.45-NA or UApoN 100× 1.49-NA tirf oil-immersion objective. Images were captured using a Photometrics Evolve512 EMCCD camera coupled to MetaMorph software (Molecular Devices).

Analysis of fluorescence intensities

Fluorescence intensity profiling was performed using Matlab (MathWorks). In brief, for each frame of an isotropically spreading cell video, a circle of radius x enclosing the entire cell was defined from cell center to edge. An actin fluorescence intensity profile was obtained along x, and the procedure was repeated for other 360 equally spaced radii (1° separation between them). These profiles were aligned according to the cell edge and then averaged across all 360 radii, creating, for each frame, a mean intensity profile. The process was repeated for all other time points to obtain the radially averaged kymograph. The same procedure was repeated for all adhesion markers (paxillin, zyxin, talin, vinculin, and VASP) used in this study. From the radially averaged kymographs, we computed D by determining the outer limit of adhesion fluorescence relative to the cell edge (defined as the outer limit of actin fluorescence).

Membrane tether extraction with optical tweezers

Tether extraction experiments were performed as previously described (Gauthier et al., 2009; Pontes et al., 2011). 1- or 3-µm-diameter concanavalin A–coated beads (Polysciences) were incubated with cells in an optical tweezers microscope (ZEISS). The optical tweezers were then used to trap a single bead and press it against a chosen cell, allowing attachment to its surface. The microscope motorized stage (Prior Scientific) was then set to move and a membrane tether was extracted. The trap calibration was achieved using the Stokes fluid friction coefficient method. By moving the sample with different velocities and measuring the respective bead center of mass displacement, the trap transverse stiffness was obtained (∼200 pN/µm). The measured bead position displacement was tracked using ImageJ and converted into measured force.

PDMS membrane wells

PDMS membranes with 30-µm-diameter wells were prepared as previously described (Masters et al., 2012). A master mold of negative pattern was incubated with PDMS and cured. The polymerized PDMS membrane was then gently peeled from the mold and directly placed on a fibronectin-coated coverslip. The set was incubated with pluronic acid to block uncoated regions, preventing cells from attaching to them. It was then mounted in a microscope chamber and transferred to the tirf microscope already described. Finally, cells were added and spread until they reached the barrier imposed by the well walls. Videos of the entire spreading process were collected with all the microscope setups already described.

Micropatterning circles

Glass coverslips were cleaned by a 5-min-interval exposure to UV-ozone (ProCleaner UV-ozone cleaner) followed by incubation with 0.1 mg/ml PLL(20)-g[3.5]-PEG(2) (SuSoS) for 1 h. The PLL-g-PEG–coated coverslips were then put in contact with UV-transparent quartz photomasks containing 40- to 45-µm-diameter circles and patterned for 5 min by UV irradiation (185- to 254-nm wavelength). Finally, the coverslips were incubated with 10 µg/ml fibronectin for 2 h at 37°C. Fibronectin selectively bound to areas without PLL-g-PEG, attaching to the 40- to 45-µm circular areas and creating adhesive surfaces for cell spreading. Cells were plated in the micropatterned coverslips and allowed to spread before being taken to the microscope.

Cell stretching/relaxation

The cell stretching/relaxation experiments were performed as previously described (Kosmalska et al., 2015). Cells were transiently transfected with membrane-GFP/actin-RFP and paxillin-RFP/actin-GFP the day before the experiment and underwent the procedures already described. 24 h later, the transfected cells were trypsinized, seeded on either normal or prestretched PDMS membranes, and allowed to spread for 30 min. The PDMS membranes with cells were placed on a stretch system attached to an upright Nikon eclipse Ni-U microscope. The stretching or relaxation experiments were performed while the behaviors of the fluorescent proteins were followed with a CFI Fluor 60× 1.0-NA water-immersion objective lens. The images were captured using an Orca Flash 4.0 camera (Hamamatsu Photonics).

Statistical analysis

All quantification values in the text are presented as mean ± standard error. Data were analyzed using Prism (GraphPad Software). *t* Tests were used to make comparisons between groups.

Computational model

Lamellipodial dynamics is simulated using a set of differential equations to describe a 1D cross section of the cell edge. The cross section is divided into discrete segments, each representing a region of actin mesh between adjacent adhesions or between the outermost adhesion and the cell edge. The actin segments were modeled as free bodies, connected visco-elastically to each other, and moving along one dimension. At the actin segment, junctions are cell-matrix-adhesion modeled as elastic links to a fixed reference point. Adhesions can be positioned at the front or disassembled at the rear, such that the model alternates between a two-segment configuration and a three-segment configuration. In addition to the segments and adhesions, the model includes a constant force pulling inward from the lamella and a membrane barrier that can apply inward force to the outermost actin segment (depending on the amount of available membrane). Scalar variables represent the rest length of each segment, analogous to the amount of actin in each segment. These scalars for the actin segments provide a coarsely discretized representation of actin dynamics: continually increasing actin in the outermost segment represents actin polymerization with elongation of the outermost segment, and transfer of actin from segment to segment represents retrograde flow. The equations and parameters are provided in the text as well as in Table 2. The differential equations are solved numerically in Matlab with an explicit Runge–Kutta method.

Table 2. **Parameters for the computational model**

Parameter	Value
	a.u.
E_{mat}	10
E (cell membrane)	0.2
η (cell membrane)	0.3
E (actin sheets)	5
η (actin sheets)	5
η (lamella)	50
p_0	0.6
ρ_{min}	0.2
ρ_{max}	0.8
f_{crit}	0.0145
$k_{\boldsymbol{\rho}}$	0.45
k_r	10
k_E	10
$\boldsymbol{\sigma}_{crit}$	0.016
L_{crit}	1

Mechanics of the lamellipodium. Fig. S5 (E and F) shows the computational model configurations for two or three adhesions, respectively. Actin segments (A1, A2, and A3) are modeled as viscoelastic solids with a linear viscous dashpot and linear elastic spring in series.

Although a lipid bilayer by itself would be relatively inelastic, we choose a spring and dashpot in series to describe the bulk mechanics of the cell membrane system, which includes vesicle transport, membrane reservoirs, and membrane unfolding. The relationship between the stress and strain of viscoelastic solids, where Young's modulus (E) is not constant, is given by the following equation:

$$\frac{d\varepsilon}{dt} - \frac{1}{E}\frac{d\sigma}{dt} + \frac{\sigma}{E^2}\frac{dE}{dt} = \frac{\sigma}{\eta},$$

where σ is the stress, ε is the strain, and η is the coefficient of viscosity.

Changes in membrane tension (whether accompanying the transition from P1 spreading to P2 spreading or induced by hypotonic shock) are implemented by applying a step increase in η and E of the cell membrane, which represents a decrease in membrane availability.

Adhesions (abbreviated FA, but including nascent adhesions as well as focal adhesions) are modeled as elastic attachments to a fixed reference, and the Young's modulus of the attachment increases after

FA maturation. The equation governing the stress and strain of elastic solids is as follows:

$$\frac{d\varepsilon}{dt} - \frac{1}{E}\frac{d\sigma}{dt} + \frac{\sigma}{E^2}\frac{dE}{dt} = 0.$$

The lamellipodium is connected through the lamella (LM) to the cell body, which is modeled as a fixed plane on the left. The lamella is represented by an inward actuator, which represents inward myosin pull, plus viscous relaxation that dampens any displacement caused by lamellipodial extension and retraction. The constitutive equation for the lamella is simply

$$\frac{d\varepsilon}{dt} = \frac{\sigma}{\eta}.$$

Cell edge protrusion. Lamellipodial protrusion is driven by actin polymerization, which increases the resting length of the outermost actin segment A1. The rate of increase in the resting length attributable to actin polymerization is $p_e = \rho(f_{mem})p_0$, where p_e is the effective protrusion rate. The effective protrusion rate is a product of constant polymerization rate p_0 and protrusion coefficient ρ. The protrusion coefficient ρ ranges between ρ_{min} and ρ_{max} (where $\rho_{min} \geq 0$ and $\rho_{max} \leq 1$) depending on the membrane tension f_{mem}. Biologically, this variable protrusion represents changes in the angular mesh of protrusive actin such that filaments are more perpendicular to the edge when membrane tension is low and more oblique to the edge when membrane tension is high. ρ is described by the following equation:

$$\frac{d\rho}{dt} = \begin{cases} k_\rho\left(\frac{\rho}{\rho_{\min}} - 1\right)\delta(\rho_{\max} - \rho) & f_{mem} < f_{crit} \\ k_\rho\left(1 - \frac{\rho}{\rho_{\max}}\right)\delta(\rho - \rho_{\min}) & f_{mem} \geq f_{crit} \end{cases},$$

where k_ρ is the rate constant, δ is the Heaviside function, and f_{crit} is the critical membrane tension. The upper expression defines the switch from ρ_{min} to ρ_{max} when f_{mem} is low, and the lower expression defines the change in ρ from ρ_{max} to ρ_{min} when f_{mem} is high.

Retrograde flow. The retrograde flow F_A at any actin segment A is caused by a combination of pushing force derived from actin polymerization against the membrane and pulling force from actomyosin contraction in the lamella. Actin treadmilling with constant lamellipodium width can therefore occur if there is a balance between polymerization and retrograde flow. Retrograde flow is computed from the stress differential between adjacent actin segments. In the two-adhesion model,

$$F_{A_1} = k_r\left(\sigma_{A_2} - \sigma_{A_1}\right)L_{A_1}$$

$$F_{A_2} = k_r\left(\sigma_{LM} - \sigma_{A_2}\right)L_{A_2}$$

and the three adhesion model,

$$F_{A_1} = k_r\left(\sigma_{A_2} - \sigma_{A_1}\right)L_{A_1}$$

$$F_{A_2} = k_r\left(\sigma_{A_3} - \sigma_{A_2}\right)L_{A_2}$$

$$F_{A_3} = k_r\left(\sigma_{LM} - \sigma_{A_3}\right)L_{A_3},$$

where L_{A_i} denotes the length of the actin segment and k_r is the rate constant for retrograde flow. Finally, the change in the actin segment resting length $L0_{A_i}$ can be calculated from the mass balance of actin:

$$\frac{dL0_{A_i}}{dt} = \begin{cases} p_e - F_{A_i} & i = 1 \\ F_{A_{i-1}} - F_{A_i} & i > 1 \end{cases}.$$

Focal adhesion dynamics. In this model, an adhesion is positioned near the cell edge whenever the membrane tension σ rises above a critical threshold σ_{crit} L_{crit}. Adhesion positioning is implemented as a transition from the two-adhesion model into the three-adhesion model. The properties (E,η) and states (σ,ε) of the three-adhesion model are taken from the two-adhesion model, and the outer two actin segments (A1 and A2) in the three-adhesion model inherit the stress, strain, and mechanical properties of the cell edge actin (A1) in the two-adhesion model. Model elements present in the three-adhesion model but not the two-adhesion model were initialized with default values. The new positioned adhesion in the three-adhesion model is initialized with zero stress, zero strain, and a small Young's modulus (E = 0.001). Subsequently, the adhesion grows, and its E increases according to the following equation:

$$\frac{dE}{dt} = k_E\delta(E - E_{mat}),$$

where k_E is the rate constant and E_{mat} is the Young's modulus of a fully mature adhesion.

After the newest positioned adhesion matures in the three-adhesion model, the innermost (oldest) adhesion is assumed to leave the scope of the model, whether by joining the lamella, disassembling, or both. To minimize discontinuity during the transition from three-adhesion to two-adhesion model, the effect of the innermost adhesion is decreased by reducing its Young's modulus E with a first-order rate constant of k_E. When the E is sufficiently small (<1.0), the model jumps discontinuously to the two-adhesion model by discarding the innermost adhesion (FA3) and actin segment (A3), and lengthening the lamella to include the space formerly occupied by A3.

Online supplemental material

Fig. S1 shows the behaviors of VASP, Arp 2/3, and cofilin during spreading. Fig. S2 shows the behavior of the activated Rac1 reporter (PBD) as well as its correlation with the membrane tension increase during spreading. Fig. S3 shows cycles of lamellipodial actin buckling in BBI-treated cells and the behavior of activated integrin β1 (stained for 9EG7 antibody) as well as its correlation with the membrane tension increase during spreading. Fig. S4 shows the behavior of actin and paxillin during lamellipodial buckling cycles in migrating cells. Fig. S5 shows the tether force of nontransfected vinculin KO cells and a schematic representation of the cell leading edge used for the computational model. Video 1 shows the behavior of VASP and actin during cell spreading. Video 2 shows the behavior of several adhesion markers during spreading. Video 3 shows the dynamics of paxillin and actin during cell spreading in control, BBI, control plus hypo-OS, and BBI plus hypo-OS. Video 4 shows the dynamics of membrane, actin, and paxillin during cell stretching in control and BBI-treated conditions as well as their dynamics during relaxation of prestretched PDMS substrates. Video 5 shows the dynamics of Arp2/3 and cofilin during spreading. Video 6 shows the correlative DIC, epi, and tirf microscopy of buckling during P2 spreading. Video 7 shows a membrane tether extraction experiment with optical tweezers in a P2 spreading cell. Video 8 shows a cell spreading inside a confined circular PDMS well, a lamellipodium protruding from a cell attached to a confined fibronectin-coated micropattern circle, and lamellipodia protruding from a cell attached to a confined fibronectin-coated micropattern circle during media exchanges. Video 9 shows the spreading dynamics of two vinculin KO cells, one transfected with vinculin full-length construct and another transfected with vinculin head-domain construct. Video 10 shows the computational model of membrane tension–mediated adhesion row positioning. A ZIP file is available that includes the files necessary to install and run the source code for imaging analysis.

Acknowledgments

We thank Michael P. Sheetz, Benoit Ladoux, Barbara Hissa, Paolo Maiuri, Víctor González, and members of Gauthier's group for help and fruitful discussions.

This work was supported by the Mechanobiology Institute (co-founded by the National Research Foundation Singapore and the Ministry of Education of Singapore), by an Istituto Fondazione Italiana per la Ricerca sul Cancro di Oncologia Molecolare (Milan, Italy) starting grant to Gauthier's group,by the Brazilian agencies Conselho Nacional de Desenvolvimento Científico and Fundação de Amparo à Pesquisa do Rio de Janeiro, by the Spanish Ministry of Economy and Competitiveness (BFU2016-79916-P), and by the European Commission (Grant Agreeement SEP-210342844).

The authors declare no competing financial interests.

Author contributions: B. Pontes and N.C. Gauthier conceived the project, designed and performed experiments, analyzed results, and wrote the manuscript. P. Monzo, W. Luo, and S. Kan performed experiments. L. Gole and V. Viasnoff contributed to image analysis tools and microfabrication. A-L. Le Roux, A.J. Kosmalska, and P. Roca-Cusachs performed experiments and contributed with expertise for cell stretching. Z.Y. Tam and L. Tucker-Kellogg developed the computational model.

Submitted: 19 November 2016
Revised: 4 April 2017
Accepted: 1 June 2017

References

Batchelder, E.L., G. Hollopeter, C. Campillo, X. Mezanges, E.M. Jorgensen, P. Nassoy, P. Sens, and J. Plastino. 2011. Membrane tension regulates motility by controlling lamellipodium organization. *Proc. Natl. Acad. Sci. USA.* 108:11429–11434. http://dx.doi.org/10.1073/pnas.1010481108

Bear, J.E., and F.B. Gertler. 2009. Ena/VASP: Towards resolving a pointed controversy at the barbed end. *J. Cell Sci.* 122:1947–1953. http://dx.doi.org/10.1242/jcs.038125

Bieling, P., T.D. Li, J. Weichsel, R. McGorty, P. Jreij, B. Huang, D.A. Fletcher, and R.D. Mullins. 2016. Force feedback controls motor activity and mechanical properties of self-assembling branched actin networks. *Cell.* 164:115–127. http://dx.doi.org/10.1016/j.cell.2015.11.057

Burnette, D.T., S. Manley, P. Sengupta, R. Sougrat, M.W. Davidson, B. Kachar, and J. Lippincott-Schwartz. 2011. A role for actin arcs in the leading-edge advance of migrating cells. *Nat. Cell Biol.* 13:371–381. http://dx.doi.org/10.1038/ncb2205

Burnette, D.T., L. Shao, C. Ott, A.M. Pasapera, R.S. Fischer, M.A. Baird, C. Der Loughian, H. Delanoe-Ayari, M.J. Paszek, M.W. Davidson, et al. 2014. A contractile and counterbalancing adhesion system controls the 3D shape of crawling cells. *J. Cell Biol.* 205:83–96. http://dx.doi.org/10.1083/jcb.201311104

Carisey, A., R. Tsang, A.M. Greiner, N. Nijenhuis, N. Heath, A. Nazgiewicz, R. Kemkemer, B. Derby, J. Spatz, and C. Ballestrem. 2013. Vinculin regulates the recruitment and release of core focal adhesion proteins in a force-dependent manner. *Curr. Biol.* 23:271–281. http://dx.doi.org/10.1016/j.cub.2013.01.009

Case, L.B., M.A. Baird, G. Shtengel, S.L. Campbell, H.F. Hess, M.W. Davidson, and C.M. Waterman. 2015. Molecular mechanism of vinculin activation and nanoscale spatial organization in focal adhesions. *Nat. Cell Biol.* 17:880–892. http://dx.doi.org/10.1038/ncb3180

Choi, C.K., M. Vicente-Manzanares, J. Zareno, L.A. Whitmore, A. Mogilner, and A.R. Horwitz. 2008. Actin and α-actinin orchestrate the assembly and maturation of nascent adhesions in a myosin II motor-independent manner. *Nat. Cell Biol.* 10:1039–1050. http://dx.doi.org/10.1038/ncb1763

Dai, J., and M.P. Sheetz. 1999. Membrane tether formation from blebbing cells. *Biophys. J.* 77:3363–3370. http://dx.doi.org/10.1016/S0006-3495(99)77168-7

Diz-Muñoz, A., D.A. Fletcher, and O.D. Weiner. 2013. Use the force: Membrane tension as an organizer of cell shape and motility. *Trends Cell Biol.* 23:47–53. http://dx.doi.org/10.1016/j.tcb.2012.09.006

Diz-Muñoz, A., K. Thurley, S. Chintamen, S.J. Altschuler, L.F. Wu, D.A. Fletcher, and O.D. Weiner. 2016. Membrane tension acts through PLD2 and mTORC2 to limit actin network assembly during neutrophil migration. *PLoS Biol.* 14:e1002474. http://dx.doi.org/10.1371/journal.pbio.1002474

Doyle, A.D., M.L. Kutys, M.A. Conti, K. Matsumoto, R.S. Adelstein, and K.M. Yamada. 2012. Micro-environmental control of cell migration—Myosin IIA is required for efficient migration in fibrillar environments through control of cell adhesion dynamics. *J. Cell Sci.* 125:2244–2256. http://dx.doi.org/10.1242/jcs.098806

Dubin-Thaler, B.J., G. Giannone, H.G. Döbereiner, and M.P. Sheetz. 2004. Nanometer analysis of cell spreading on matrix-coated surfaces reveals two distinct cell states and STEPs. *Biophys. J.* 86:1794–1806. http://dx.doi.org/10.1016/S0006-3495(04)74246-0

Dubin-Thaler, B.J., J.M. Hofman, Y. Cai, H. Xenias, I. Spielman, A.V. Shneidman, L.A. David, H.G. Döbereiner, C.H. Wiggins, and M.P. Sheetz. 2008. Quantification of cell edge velocities and traction forces reveals distinct motility modules during cell spreading. *PLoS One.* 3:e3735. http://dx.doi.org/10.1371/journal.pone.0003735

Dumbauld, D.W., T.T. Lee, A. Singh, J. Scrimgeour, C.A. Gersbach, E.A. Zamir, J. Fu, C.S. Chen, J.E. Curtis, S.W. Craig, and A.J. García. 2013. How vinculin regulates force transmission. *Proc. Natl. Acad. Sci. USA.* 110:9788–9793. http://dx.doi.org/10.1073/pnas.1216209110

Gabella, C., E. Bertseva, C. Bottier, N. Piacentini, A. Bornert, S. Jeney, L. Forró, I.F. Sbalzarini, J.J. Meister, and A.B. Verkhovsky. 2014. Contact angle at the leading edge controls cell protrusion rate. *Curr. Biol.* 24:1126–1132. http://dx.doi.org/10.1016/j.cub.2014.03.050

Gauthier, N.C., O.M. Rossier, A. Mathur, J.C. Hone, and M.P. Sheetz. 2009. Plasma membrane area increases with spread area by exocytosis of a GPI-anchored protein compartment. *Mol. Biol. Cell.* 20:3261–3272. http://dx.doi.org/10.1091/mbc.E09-01-0071

Gauthier, N.C., M.A. Fardin, P. Roca-Cusachs, and M.P. Sheetz. 2011. Temporary increase in plasma membrane tension coordinates the activation of exocytosis and contraction during cell spreading. *Proc. Natl. Acad. Sci. USA.* 108:14467–14472. http://dx.doi.org/10.1073/pnas.1105845108

Gauthier, N.C., T.A. Masters, and M.P. Sheetz. 2012. Mechanical feedback between membrane tension and dynamics. *Trends Cell Biol.* 22:527–535. http://dx.doi.org/10.1016/j.tcb.2012.07.005

Giannone, G., B.J. Dubin-Thaler, H.G. Döbereiner, N. Kieffer, A.R. Bresnick, and M.P. Sheetz. 2004. Periodic lamellipodial contractions correlate with rearward actin waves. *Cell.* 116:431–443. http://dx.doi.org/10.1016/S0092-8674(04)00058-3

Giannone, G., B.J. Dubin-Thaler, O. Rossier, Y. Cai, O. Chaga, G. Jiang, W. Beaver, H.G. Döbereiner, Y. Freund, G. Borisy, and M.P. Sheetz. 2007. Lamellipodial actin mechanically links myosin activity with adhesion-site formation. *Cell.* 128:561–575. http://dx.doi.org/10.1016/j.cell.2006.12.039

Houk, A.R., A. Jilkine, C.O. Mejean, R. Boltyanskiy, E.R. Dufresne, S.B. Angenent, S.J. Altschuler, L.F. Wu, and O.D. Weiner. 2012. Membrane tension maintains cell polarity by confining signals to the leading edge during neutrophil migration. *Cell.* 148:175–188. http://dx.doi.org/10.1016/j.cell.2011.10.050

Hu, K., L. Ji, K.T. Applegate, G. Danuser, and C.M. Waterman-Storer. 2007. Differential transmission of actin motion within focal adhesions. *Science.* 315:111–115. http://dx.doi.org/10.1126/science.1135085

Ichetovkin, I., W. Grant, and J. Condeelis. 2002. Cofilin produces newly polymerized actin filaments that are preferred for dendritic nucleation by the Arp2/3 complex. *Curr. Biol.* 12:79–84. http://dx.doi.org/10.1016/S0960-9822(01)00629-7

Ji, L., J. Lim, and G. Danuser. 2008. Fluctuations of intracellular forces during cell protrusion. *Nat. Cell Biol.* 10:1393–1400. http://dx.doi.org/10.1038/ncb1797

Keren, K. 2011. Cell motility: The integrating role of the plasma membrane. *Eur. Biophys. J.* 40:1013–1027. http://dx.doi.org/10.1007/s00249-011-0741-0

Keren, K., Z. Pincus, G.M. Allen, E.L. Barnhart, G. Marriott, A. Mogilner, and J.A. Theriot. 2008. Mechanism of shape determination in motile cells. *Nature.* 453:475–480. http://dx.doi.org/10.1038/nature06952

Kosmalska, A.J., L. Casares, A. Elosegui-Artola, J.J. Thottacherry, R. Moreno-Vicente, V. González-Tarragó, M.A. del Pozo, S. Mayor, M. Arroyo, D. Navajas, et al. 2015. Physical principles of membrane remodelling during cell mechanoadaptation. *Nat. Commun.* 6:7292. http://dx.doi.org/10.1038/ncomms8292

Kozlov, M.M., and A. Mogilner. 2007. Model of polarization and bistability of cell fragments. *Biophys. J.* 93:3811–3819. http://dx.doi.org/10.1529/biophysj.107.110411

Lacayo, C.I., Z. Pincus, M.M. VanDuijn, C.A. Wilson, D.A. Fletcher, F.B. Gertler, A. Mogilner, and J.A. Theriot. 2007. Emergence of large-

scale cell morphology and movement from local actin filament growth dynamics. *PLoS Biol.* 5:e233. http://dx.doi.org/10.1371/journal.pbio.0050233

Le Clainche, C., and M.F. Carlier. 2008. Regulation of actin assembly associated with protrusion and adhesion in cell migration. *Physiol. Rev.* 88:489–513. http://dx.doi.org/10.1152/physrev.00021.2007

Lieber, A.D., S. Yehudai-Resheff, E.L. Barnhart, J.A. Theriot, and K. Keren. 2013. Membrane tension in rapidly moving cells is determined by cytoskeletal forces. *Curr. Biol.* 23:1409–1417. http://dx.doi.org/10.1016/j.cub.2013.05.063

Lieber, A.D., Y. Schweitzer, M.M. Kozlov, and K. Keren. 2015. Front-to-rear membrane tension gradient in rapidly moving cells. *Biophys. J.* 108:1599–1603. http://dx.doi.org/10.1016/j.bpj.2015.02.007

Lo, C.M., D.B. Buxton, G.C. Chua, M. Dembo, R.S. Adelstein, and Y.L. Wang. 2004. Nonmuscle myosin IIb is involved in the guidance of fibroblast migration. *Mol. Biol. Cell.* 15:982–989. http://dx.doi.org/10.1091/mbc.E03-06-0359

Machacek, M., L. Hodgson, C. Welch, H. Elliott, O. Pertz, P. Nalbant, A. Abell, G.L. Johnson, K.M. Hahn, and G. Danuser. 2009. Coordination of Rho GTPase activities during cell protrusion. *Nature.* 461:99–103. http://dx.doi.org/10.1038/nature08242

Masters, T., W. Engl, Z.L. Weng, B. Arasi, N. Gauthier, and V. Viasnoff. 2012. Easy fabrication of thin membranes with through holes. Application to protein patterning. *PLoS One.* 7:e44261. http://dx.doi.org/10.1371/journal.pone.0044261

Masters, T.A., B. Pontes, V. Viasnoff, Y. Li, and N.C. Gauthier. 2013. Plasma membrane tension orchestrates membrane trafficking, cytoskeletal remodeling, and biochemical signaling during phagocytosis. *Proc. Natl. Acad. Sci. USA.* 110:11875–11880. http://dx.doi.org/10.1073/pnas.1301766110

McGough, A., B. Pope, W. Chiu, and A. Weeds. 1997. Cofilin changes the twist of F-actin: Implications for actin filament dynamics and cellular function. *J. Cell Biol.* 138:771–781. http://dx.doi.org/10.1083/jcb.138.4.771

Meacci, G., H. Wolfenson, S. Liu, M.R. Stachowiak, T. Iskratsch, A. Mathur, S. Ghassemi, N. Gauthier, E. Tabdanov, J. Lohner, et al. 2016. α-Actinin links extracellular matrix rigidity-sensing contractile units with periodic cell-edge retractions. *Mol. Biol. Cell.* 27:3471–3479. http://dx.doi.org/10.1091/mbc.E16-02-0107

Morris, C.E., and U. Homann. 2001. Cell surface area regulation and membrane tension. *J. Membr. Biol.* 179:79–102. http://dx.doi.org/10.1007/s002320010040

Mullins, R.D., J.A. Heuser, and T.D. Pollard. 1998. The interaction of Arp2/3 complex with actin: Nucleation, high affinity pointed end capping, and formation of branching networks of filaments. *Proc. Natl. Acad. Sci. USA.* 95:6181–6186. http://dx.doi.org/10.1073/pnas.95.11.6181

Nagae, M., S. Re, E. Mihara, T. Nogi, Y. Sugita, and J. Takagi. 2012. Crystal structure of α5β1 integrin ectodomain: Atomic details of the fibronectin receptor. *J. Cell Biol.* 197:131–140. http://dx.doi.org/10.1083/jcb.201111077

Nassoy, P., and C. Lamaze. 2012. Stressing caveolae new role in cell mechanics. *Trends Cell Biol.* 22:381–389. http://dx.doi.org/10.1016/j.tcb.2012.04.007

Oliver, T., M. Dembo, and K. Jacobson. 1999. Separation of propulsive and adhesive traction stresses in locomoting keratocytes. *J. Cell Biol.* 145:589–604. http://dx.doi.org/10.1083/jcb.145.3.589

Parsons, J.T., A.R. Horwitz, and M.A. Schwartz. 2010. Cell adhesion: Integrating cytoskeletal dynamics and cellular tension. *Nat. Rev. Mol. Cell Biol.* 11:633–643. http://dx.doi.org/10.1038/nrm2957

Plançon, S., M.C. Morel-Kopp, E. Schaffner-Reckinger, P. Chen, and N. Kieffer. 2001. Green fluorescent protein (GFP) tagged to the cytoplasmic tail of αIIb or β3 allows the expression of a fully functional integrin αIIb(β3): Effect of β3GFP on αIIb(β3) ligand binding. *Biochem. J.* 357:529–536. http://dx.doi.org/10.1042/bj3570529

Pollard, T.D., and G.G. Borisy. 2003. Cellular motility driven by assembly and disassembly of actin filaments. *Cell.* 112:453–465. http://dx.doi.org/10.1016/S0092-8674(03)00120-X

Pontes, B., N.B. Viana, L.T. Salgado, M. Farina, V. Moura Neto, and H.M. Nussenzveig. 2011. Cell cytoskeleton and tether extraction. *Biophys. J.* 101:43–52. http://dx.doi.org/10.1016/j.bpj.2011.05.044

Pontes, B., Y. Ayala, A.C. Fonseca, L.F. Romão, R.F. Amaral, L.T. Salgado, F.R. Lima, M. Farina, N.B. Viana, V. Moura-Neto, and H.M. Nussenzveig. 2013. Membrane elastic properties and cell function. *PLoS One.* 8:e67708. http://dx.doi.org/10.1371/journal.pone.0067708

Prass, M., K. Jacobson, A. Mogilner, and M. Radmacher. 2006. Direct measurement of the lamellipodial protrusive force in a migrating cell. *J. Cell Biol.* 174:767–772. http://dx.doi.org/10.1083/jcb.200601159

Raucher, D., and M.P. Sheetz. 2000. Cell spreading and lamellipodial extension rate is regulated by membrane tension. *J. Cell Biol.* 148:127–136. http://dx.doi.org/10.1083/jcb.148.1.127

Reuzeau, C., L.R. Mills, J.A. Harris, and C.E. Morris. 1995. Discrete and reversible vacuole-like dilations induced by osmomechanical perturbation of neurons. *J. Membr. Biol.* 145:33–47. http://dx.doi.org/10.1007/BF00233305

Risca, V.I., E.B. Wang, O. Chaudhuri, J.J. Chia, P.L. Geissler, and D.A. Fletcher. 2012. Actin filament curvature biases branching direction. *Proc. Natl. Acad. Sci. USA.* 109:2913–2918. http://dx.doi.org/10.1073/pnas.1114292109

Rottner, K., B. Behrendt, J.V. Small, and J. Wehland. 1999. VASP dynamics during lamellipodia protrusion. *Nat. Cell Biol.* 1:321–322. http://dx.doi.org/10.1038/13040

Schweitzer, Y., A.D. Lieber, K. Keren, and M.M. Kozlov. 2014. Theoretical analysis of membrane tension in moving cells. *Biophys. J.* 106:84–92. http://dx.doi.org/10.1016/j.bpj.2013.11.009

Sens, P., and J. Plastino. 2015. Membrane tension and cytoskeleton organization in cell motility. *J. Phys. Condens. Matter.* 27:273103. http://dx.doi.org/10.1088/0953-8984/27/27/273103

Shemesh, T., A.D. Bershadsky, and M.M. Kozlov. 2012. Physical model for self-organization of actin cytoskeleton and adhesion complexes at the cell front. *Biophys. J.* 102:1746–1756. http://dx.doi.org/10.1016/j.bpj.2012.03.006

Sinha, B., D. Köster, R. Ruez, P. Gonnord, M. Bastiani, D. Abankwa, R.V. Stan, G. Butler-Browne, B. Vedie, L. Johannes, et al. 2011. Cells respond to mechanical stress by rapid disassembly of caveolae. *Cell.* 144:402–413. http://dx.doi.org/10.1016/j.cell.2010.12.031

Straight, A.F., A. Cheung, J. Limouze, I. Chen, N.J. Westwood, J.R. Sellers, and T.J. Mitchison. 2003. Dissecting temporal and spatial control of cytokinesis with a myosin II inhibitor. *Science.* 299:1743–1747. http://dx.doi.org/10.1126/science.1081412

Svitkina, T.M., and G.G. Borisy. 1999. Arp2/3 complex and actin depolymerizing factor/cofilin in dendritic organization and treadmilling of actin filament array in lamellipodia. *J. Cell Biol.* 145:1009–1026. http://dx.doi.org/10.1083/jcb.145.5.1009

Theriot, J.A., and T.J. Mitchison. 1991. Actin microfilament dynamics in locomoting cells. *Nature.* 352:126–131. http://dx.doi.org/10.1038/352126a0

Thievessen, I., P.M. Thompson, S. Berlemont, K.M. Plevock, S.V. Plotnikov, A. Zemljic-Harpf, R.S. Ross, M.W. Davidson, G. Danuser, S.L. Campbell, and C.M. Waterman. 2013. Vinculin-actin interaction couples actin retrograde flow to focal adhesions, but is dispensable for focal adhesion growth. *J. Cell Biol.* 202:163–177. http://dx.doi.org/10.1083/jcb.201303129

Trichet, L., C. Sykes, and J. Plastino. 2008. Relaxing the actin cytoskeleton for adhesion and movement with Ena/VASP. *J. Cell Biol.* 181:19–25. http://dx.doi.org/10.1083/jcb.200710168

Tsujita, K., T. Takenawa, and T. Itoh. 2015. Feedback regulation between plasma membrane tension and membrane-bending proteins organizes cell polarity during leading edge formation. *Nat. Cell Biol.* 17:749–758. http://dx.doi.org/10.1038/ncb3162

Vicente-Manzanares, M., J. Zareno, L. Whitmore, C.K. Choi, and A.F. Horwitz. 2007. Regulation of protrusion, adhesion dynamics, and polarity by myosins IIA and IIB in migrating cells. *J. Cell Biol.* 176:573–580. http://dx.doi.org/10.1083/jcb.200612043

Weed, S.A., A.V. Karginov, D.A. Schafer, A.M. Weaver, A.W. Kinley, J.A. Cooper, and J.T. Parsons. 2000. Cortactin localization to sites of actin assembly in lamellipodia requires interactions with F-actin and the Arp2/3 complex. *J. Cell Biol.* 151:29–40. http://dx.doi.org/10.1083/jcb.151.1.29

Yu, C.H., J.B. Law, M. Suryana, H.Y. Low, and M.P. Sheetz. 2011. Early integrin binding to Arg-Gly-Asp peptide activates actin polymerization and contractile movement that stimulates outward translocation. *Proc. Natl. Acad. Sci. USA.* 108:20585–20590. http://dx.doi.org/10.1073/pnas.1109485108

Zhang, X., G. Jiang, Y. Cai, S.J. Monkley, D.R. Critchley, and M.P. Sheetz. 2008. Talin depletion reveals independence of initial cell spreading from integrin activation and traction. *Nat. Cell Biol.* 10:1062–1068. http://dx.doi.org/10.1038/ncb1765